© 2021. Published by The Company of Biologists Ltd | Development (2021) 148, dev196295. doi:10.1242/dev.196295

RESEARCH ARTICLE

MFN2 interacts with nuage-associated proteins and is essential for male germ cell development by controlling mRNA fate during spermatogenesis

Xiaoli Wang[1], Yujiao Wen[1], Jin Zhang[1], Grace Swanson[2], Shuangshuang Guo[1], Congcong Cao[1], Stephen A. Krawetz[2], Zhibing Zhang[2,3] and Shuiqiao Yuan[1,4,*]

ABSTRACT

Mitochondria play a crucial role in spermatogenesis and are regulated by several mitochondrial fusion proteins. However, their functional importance associated with their structure formation and mRNA fate regulation during spermatogenesis remains unclear. Here, we show that mitofusin 2 (MFN2), a mitochondrial fusion protein, interacts with nuage-associated proteins (including MIWI, DDX4, TDRKH and GASZ) in mice. Conditional mutation of *Mfn2* in postnatal germ cells results in male sterility due to germ cell developmental defects. Moreover, MFN2 interacts with MFN1, another mitochondrial fusion protein with a high-sequence similarity to MFN2, in testes to facilitate spermatogenesis. Simultaneous mutation of *Mfn1* and *Mfn2* in testes causes very severe infertile phenotypes. Importantly, we show that MFN2 is enriched in polysome fractions of testes and interacts with MSY2, a germ cell-specific DNA/RNA-binding protein, to control gamete-specific mRNA (such as *Spata19*) translational activity during spermatogenesis. Collectively, our findings demonstrate that MFN2 interacts with nuage-associated proteins and MSY2 to regulate male germ cell development by controlling several gamete-specific mRNA fates.

KEY WORDS: Nuage proteins, Mitofusins, MSY2, Spermatogenesis, Mice

INTRODUCTION

Mitochondria are dynamic organelles that play crucial roles in multiple biological processes, including energy generation, calcium homeostasis, signal transduction, redox homeostasis and apoptosis (Chen and Chan, 2004; Westermann, 2010). Emerging evidence indicates that mitochondrial function is a crucial determinant of spermatogenesis and male fertility (Ren et al., 2019; Zhang et al., 2016). Moreover, the mitochondria and endoplasmic reticulum (ER) form contacts called mitochondria-associated ER membranes (MAMs), which are reported to be essential for supporting cell structural and functional inter-organelle communications in multiple organs, including the brain, liver and skeletal muscle (Paillusson et al., 2016; Poston et al., 2013; Rieusset, 2018; Theurey et al., 2016). Alteration of MAMs was reported in several human diseases, highlighted by neurodegenerative diseases (Paillusson et al., 2016). Interestingly, our previous work has demonstrated an abundance of MAMs in mouse and human testes and identified a large portion of MAM proteins in testicular cells (Wang et al., 2018), suggesting that MAM proteins may have essential functions in spermatogenesis and male fertility.

Mitofusins (MFN1/2), the ortholog of Fzo in yeast and *Drosophila*, are the crucial regulators of mitochondrial fusion in mammalian cells and enriched in MAMs (Hales and Fuller, 1997; Santel and Fuller, 2001; Wang et al., 2018). Loss of either *Mfn1* or *Mfn2* in mice leads to embryonic lethality, and cultured cells obtained from the mutant mouse embryos display overtly fragmented mitochondria (Chen et al., 2003). Specific ablation of *Mfn2* in anorexigenic pro-opiomelanocortin (POMC) neurons in the hypothalamus results in aberrant MAMs, defective POMC processing, ER stress-induced leptin resistance, hyperphagia and obesity (Schneeberger et al., 2013). Interestingly, the mutations in human MFN2, but not MFN1, leads to Charcot–Marie–Tooth disease type 2A, a neurodegenerative disorder characterized by progressive sensory and motor loss in the limbs (Bouhy and Timmerman, 2013; Chen et al., 2007; Misko et al., 2012; Rouzier et al., 2012; Züchner et al., 2004). In addition, conditional knockout of *Mfn1*, but not *Mfn2*, in growing oocytes results in female infertility (Hou et al., 2019). Although MFN1/2 deficiency in male germ cells leads to mitochondrial defects and male infertility (Chen et al., 2020; Varuzhanyan et al., 2019; Zhang et al., 2016), the underlying mechanism of how mitofusins regulate spermatogenesis and post-meiotic male germ cell development remains largely unknown.

During spermatogenesis, multiple specific germinal structures, termed nuage, are present in the cytoplasm of male germ cells; these are electron-dense, non-membranous structures, close to mitochondria and/or nuclei. They are of varying size, yielding to different compartments that harbor different components. These primarily include the inter-mitochondrial cement (IMC), piP-body, and chromatoid body (CB) (Aravin et al., 2009; Eddy, 1974, 1975). The IMC and CB are tightly associated with mitochondria. IMC clusters formed between mitochondria are present in gonocytes, prospermatogonia, spermatogonia and meiotic spermatocytes until late pachytene spermatocytes (PS) (Eddy, 1974, 1975). The cytoplasmic IMC is considered the primary site for Piwi-interacting RNA (piRNA) pathway proteins, also known as pi-body (Aravin et al., 2009; van der Heijden et al., 2010). The chromatoid body first appears as thick cytoplasmic fibers and granulated material in the interstices of mitochondrial clusters and the perinuclear area of late PS, condenses into a single lobulated, perinuclear granule in round spermatids (RS) and disassembles later during spermatid elongation (Eddy, 1970, 1974; Fawcett et al., 1970). Several proteins have been identified and localized to the nuage, such as MIWI (also known as

[1]Institute of Reproductive Health, Tongji Medical College, Huazhong University of Science and Technology, Wuhan, Hubei 430030, China. [2]Department of Obstetrics & Gynecology, Wayne State University, Detroit, MI 48201, USA. [3]Department of Physiology, Wayne State University, Detroit, MI 48201, USA. [4]Shenzhen Huazhong University of Science and Technology Research Institute, Shenzhen, Guangdong 518057, China.

*Author for correspondence (shuiqiaoyuan@hust.edu.cn)

S.Y., 0000-0003-1460-7682

Handling Editor: Haruhiko Koseki
Received 21 August 2020; Accepted 26 February 2021

Development (2021) 148, dev196295. doi:10.1242/dev.196295

Piwil1), DDX4, MAEL, TDRKH and GASZ (Asz1) (Wang et al., 2020). Interestingly, MIWI, DDX4 and MAEL are expressed in both IMC and CB, whereas TDRKH and GASZ localize only to the IMC (Ma et al., 2009; Saxe et al., 2013; Takebe et al., 2013; Toyooka et al., 2000). Importantly, GASZ interacts with MFN1 to mediate spermatogenesis (Zhang et al., 2016). The nuage is the proposed site of germ cell functions with multiple RNA processing events, including translational regulation, RNA-mediated gene silencing, mRNA degradation, piRNA biogenesis and nonsense-mediated mRNA decay (Kotaja and Sassone-Corsi, 2007; Wang et al., 2020). Translational regulatory proteins such as MIWI, TDRD6 and MAEL have been found to be localized to the chromatoid body and associated with mRNA translational machinery and piRNA biogenesis (Castañeda et al., 2014; Fanourgakis et al., 2016; Grivna et al., 2006; Takebe et al., 2013; Vasileva et al., 2009). Thus, many components necessary for transcript processing are physically connected to the nuage during spermatogenesis.

In mice, spermatogenesis undergoes two rounds of transcriptional cessations: one is during meiosis, which includes the synapsis, desynapsis and meiotic sex chromosome inactivation (MSCI), and the other is the process in which histones are replaced by transition proteins, protamines, during late spermiogenesis (Sassone-Corsi, 2002; Wykes and Krawetz, 2003). During transcriptional cessations, a large number of germ cell-specific mRNAs are synthesized and stored in germ cells (meiotic spermatocytes or elongating spermatids) before their translation (Braun, 1998). Post-transcriptional and translational regulation of stored mRNAs ensures timely synthesis of proteins essential for male germ cell development (Braun, 1998; Kleene, 2013). For example, Y-box proteins FRGY2 (*Xenopus*)/MSY2 (mouse) (also known as YBX2), have been identified to play an essential role in the regulation of transcription and mRNA storage/translational delay in germ cells by a Y-box promoter-bound mechanism preferentially (Matsumoto and Wolffe, 1998; Yang et al., 2005a). However, limited knowledge exists about the specific regulators and how this regulation is achieved in male germ cells.

In this study, we report that MFN2, a mitochondrial fusion protein, interacts with nuage-associated proteins, including MIWI, DDX4, GASZ and TDRKH in germ cells and is essential for male germ cell development. The conditional knockout of *Mfn2* in mice led to male sterility characterized by mitochondria defects, structurally abnormal MAMs and precocious transcriptional/translational processes in germ cells. We further revealed that MFN2 interacts with MSY2 to control the fate of MSY2-bound mRNAs in testes, such as the early-translated SPATA19. Collectively, our findings uncovered a novel role for MFN2 in mitochondria-associated germinal structure formation and regulation of the spermatogenic mRNA fates during male germ cell development and spermatogenesis.

RESULTS

Expression and localization of MFN2 in male germ cells during spermatogenesis

Although MFN2 is a ubiquitously expressed protein located on both the outer mitochondrial membrane (OMM) and the ER surface in mammalian cells (de Brito and Scorrano, 2008), to date no information is available on the pattern of its expression in male germ cells during spermatogenesis. By performing RT-qPCR and western blot assays, both *Mfn2* mRNA and protein were detected in mouse testes (Fig. S1A,B) and expressed from postnatal day (P) 0 to P56 (Fig. S1C,D). Immunofluorescence staining of MFN2 in the developing testes further revealed that MFN2 is primarily expressed in prospermatogonia at P0 and spermatogonia at P7, and finally highly expressed in PS and RS at P14 to P28 (Fig. S1E).

Subcellular localization of MFN2 during spermatogenesis was determined by immunostaining in adult testes. We observed the presence of MFN2 throughout most of the germ cell development, including the mitotic spermatogonia, meiotic spermatocytes (pre-leptotene to diplotene), and RS (Fig. 1A). Interestingly, MFN2 expression was relatively high in the cytoplasm of PS and RS (Fig. 1A,B). To further determine the expression pattern of MFN2 in male germ cells, we co-stained MFN2 and GCNA1 (GCNA; a germ cell marker) in adult WT testes, and found that MFN2 distributes in almost all types of germ cells, but is nearly imperceptible in Sertoli cells (Fig. S1F). This observation was further confirmed in different isolated testicular cells by RT-qPCR and western blot assays (Fig. S1G-I). As *Mfn2* encodes an OMM protein, we confirmed its co-localization with ATP5A (an OMM marker) in adult testes by co-immunofluorescence staining (Fig. 1C). Together, these data indicate that MFN2 is highly expressed in the cytoplasm of meiotic spermatocytes and post-meiotic RS and may play an essential role in spermatogenesis.

Loss of MFN2 in postnatal germ cells leads to male sterility

To elucidate the physiological role of MFN2 in spermatogenesis, we generated germline-specific knockout mice. We used *Stra8*-Cre transgenic mice, in which Cre is expressed in undifferentiated spermatogonia at P3 (Sadate-Ngatchou et al., 2008), to delete exon 6 of the *Mfn2* gene (Fig. S2A). The efficiency of this *Mfn2* conditional knockout mouse (*Stra8-Cre; Mfn2*$^{loxp/Del}$, herein called *Mfn2*-cKO) was verified by determining levels of *Mfn2* mRNA and protein in testes. Both *Mfn2* mRNA and protein were dramatically reduced in *Mfn2*-cKO testes compared with that of control testes (Fig. 2A-D). Thus, we successfully generated the male germ cell-specific *Mfn2* mutants.

Although *Mfn2*-cKO males were viable and appeared to be grossly normal, they displayed sterility after mating with fertility-proven adult wild-type (WT) females for 5 months (zero out of six male mice were fertile). Consistent with this infertile phenotype, the testes from *Mfn2*-cKO mice were significantly smaller than their control littermates (Fig. 2E). The ratio of testis weight/body weight of *Mfn2*-cKO mice was decreased substantially at various ages, from P35 to P120, compared with controls (Fig. 2F). Histological analyses showed that, as the adult *Mfn2*-cKO mice aged, the number of severely atrophic abnormal seminiferous tubules increased (Fig. 2G), suggesting that spermatogenic defects are age-dependent in *Mfn2*-cKO mice. Interestingly, when the first wave of spermatogenesis culminated at P42, the late-stage spermatocytes and RS continually decreased in number and appeared to gradually vacuolize (Fig. 2G). In comparison, no discernible abnormality was found in the *Mfn2*-cKO testes from P7 to P28 (Fig. S2B). Consistent with these histological results, the TUNEL assay revealed that the number of apoptotic cells in *Mfn2*-cKO testes at P14 to P28 was comparable with control testes but increased significantly at P35 and P56 (Fig. S2C,D). Moreover, the number of spermatozoa retrieved from adult *Mfn2*-cKO cauda epididymis was dramatically reduced compared with controls (Fig. 2H,I). Only ∼2% of *Mfn2*-cKO epididymal sperm showed normal morphology, compared with ∼80% of the sperm in controls (Fig. 2J,K). These data indicate that, upon *Mfn2* deletion in postnatal testes, most germ cells are gradually lost from P35 by apoptosis, and the remainder is morphologically defective.

MFN2 interacts with MFN1 in testes and contributes to male fertility

MFN1 and MFN2 are the two Fzo homologs in humans and mice. They interact with each other in mammalian cells to coordinately regulate mitochondrial fusion (Chen et al., 2003), raising the question of whether MFN1 and MFN2 interact in testicular cells. We first

Development (2021) 148, dev196295. doi:10.1242/dev.196295

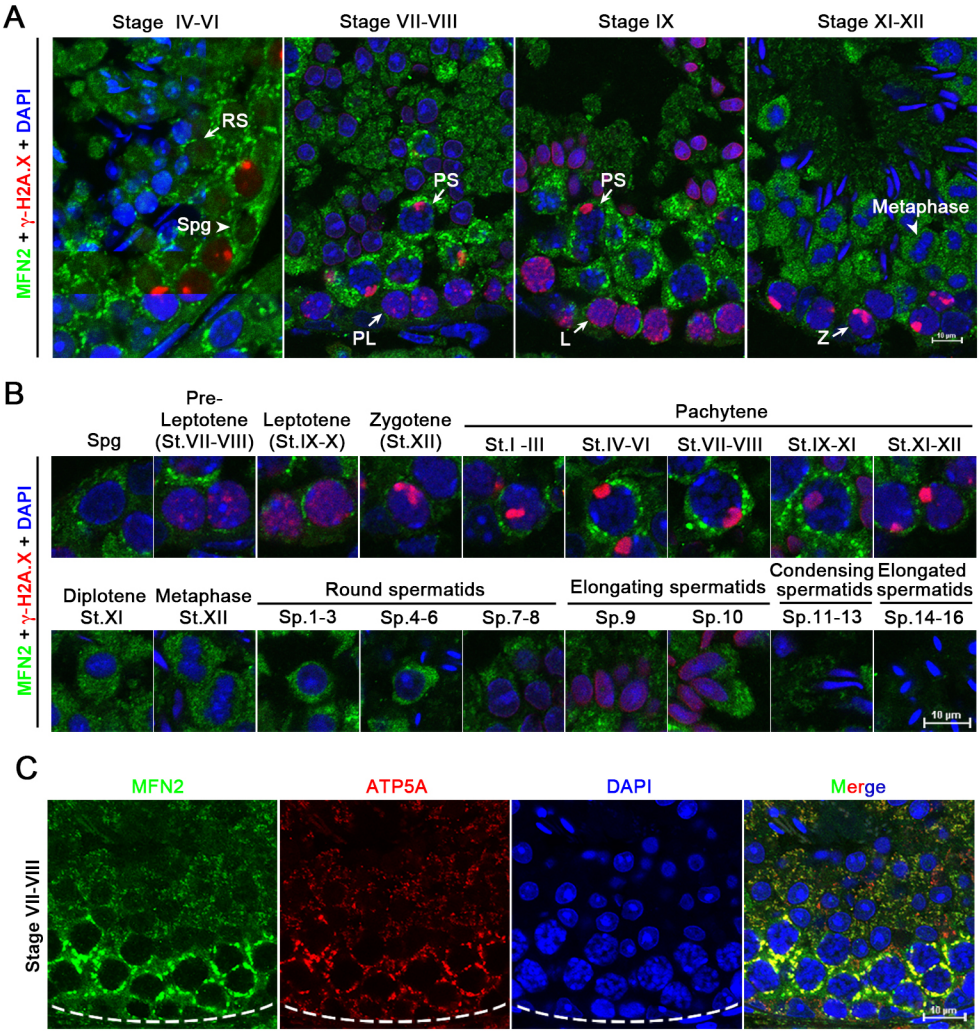

Fig. 1. MFN2 displays a dynamic expression profile during spermatogenesis. (A) Representative images of MFN2 and γ-H2A.X immunostaining on WT adult testis sections in different stages of seminiferous tubules. (B) Immunostaining of MFN2 and γ-H2A.X on different types of spermatogenic cells. (C) Co-immunostaining of MFN2 and ATP5A (an OMM marker) in stage VII-VIII seminiferous tubule from WT testes. L, leptotene spermatocytes; PL, preleptotene spermatocytes; PS, pachytene spermatocytes; RS, round spermatids; Spg, spermatogonia; Z, zygotene spermatocytes. Scale bars: 10 µm.

examined their interaction in adult mouse testes by MFN1 and MFN2 co-immunoprecipitation (Co-IP). In both the MFN2 and MFN1 antibody immunoprecipitants, each protein was detected in testes (Fig. S3A). These results confirmed that MFN1 and MFN2 are indeed bona fide interacting partners in the testes. In contrast, both MAEL (a piP-body component; Soper et al., 2008; Takebe et al., 2013) and GAPDH were not detected in the MFN2 antibody immunoprecipitants (Fig. S3B), confirming the high specificity of MFN2 antibody in Co-IP assays. To determine the role of MFN1 during spermatogenesis and male germ cell development, we then generated *Stra8*-Cre-mediated *Mfn1* conditional knockout mice through the deletion of exon 4 (*Stra8-Cre; Mfn1*$^{loxp/Del}$, herein called *Mfn1*-cKO) of the *Mfn1* gene (Fig. S3C). As expected, *Mfn1*-cKO mice were also infertile. Spermatogenesis was disrupted as evidenced by smaller testes, decreased testis weight and disrupted seminiferous tubule structure (Fig. S3D-G). Importantly, we observed that *Mfn1*-cKO testes exhibited severe vacuolization defects as early as P28. In comparison, the first wave of spermatogenesis in *Mfn2*-cKO testes proceeded normally until P42. This disparity between *Mfn1*-cKO and *Mfn2*-cKO mouse phenotypes shows that MFN2 and MFN1 are essential for spermatogenesis but each has a distinct role.

To better understand the physiological roles of mitofusins in spermatogenesis, we next simultaneously deleted *Mfn1* and *Mfn2* in mouse testis using *Stra8*-Cre-mediated Cre-Loxp strategy (*Stra8-Cre; Mfn1*$^{loxp/Del}$*-Mfn2*$^{loxp/Del}$, herein called *Mfn1/2*-cDKO). Notably, the testicular disruption in *Mfn1/2*-cDKO mice was much more severe than in either single *Mfn1* or *Mfn2*-cKO mice (Fig. 2L). Compared with the control mice, the diameters of seminiferous tubules from *Mfn1/2*-cDKO mice appeared to be much smaller, as early as P14 (Fig. S4A,B). Almost no RS were observed in *Mfn1/2*-cDKO testes at P25 (Fig. 2L). These data indicate that *Mfn1/2*-cDKO mice failed to complete meiosis, which is consistent with a previous report (Varuzhanyan et al., 2019). Consistent with the expected phenotype, the adult *Mfn1/2*-cDKO testis was much smaller than that of adult *Mfn1* or *Mfn2* single cKO mice (Fig. S4C,D). Histological analyses of adult testicular sections further revealed increased atrophic and vacuolated seminiferous tubules in *Mfn1/2*-cDKO testes compared with single *Mfn1* or *Mfn2*-cKO testes (Fig. S4E). Strikingly, unlike the uniformly distributed donut of mitochondria in the control cytoplasm, mitochondria were aggregated to one side of the cytoplasm in the *Mfn1/2*-cDKO spermatocytes at P25 (Fig. 2M; Fig. S4F). However, this abnormal mitochondria distribution was not observed in *Mfn1*-cKO or *Mfn2*-cKO mice (Fig. S4F). Together, these results suggest that MFN2 could interact with MFN1 to regulate the distribution of mitochondria in the testes, thereby contributing to spermatogenesis and male germ cell development.

Ablation of MFN2, but not MFN1, in testes disrupts the MAM and ER structures in male germ cells

Given that the distribution of the mitochondria was disrupted in *Mfn1/2*-cDKO testes, we examined the ultrastructure of mitochondria and its associated organelles (MAMs and ER) in

Development (2021) 148, dev196295. doi:10.1242/dev.196295

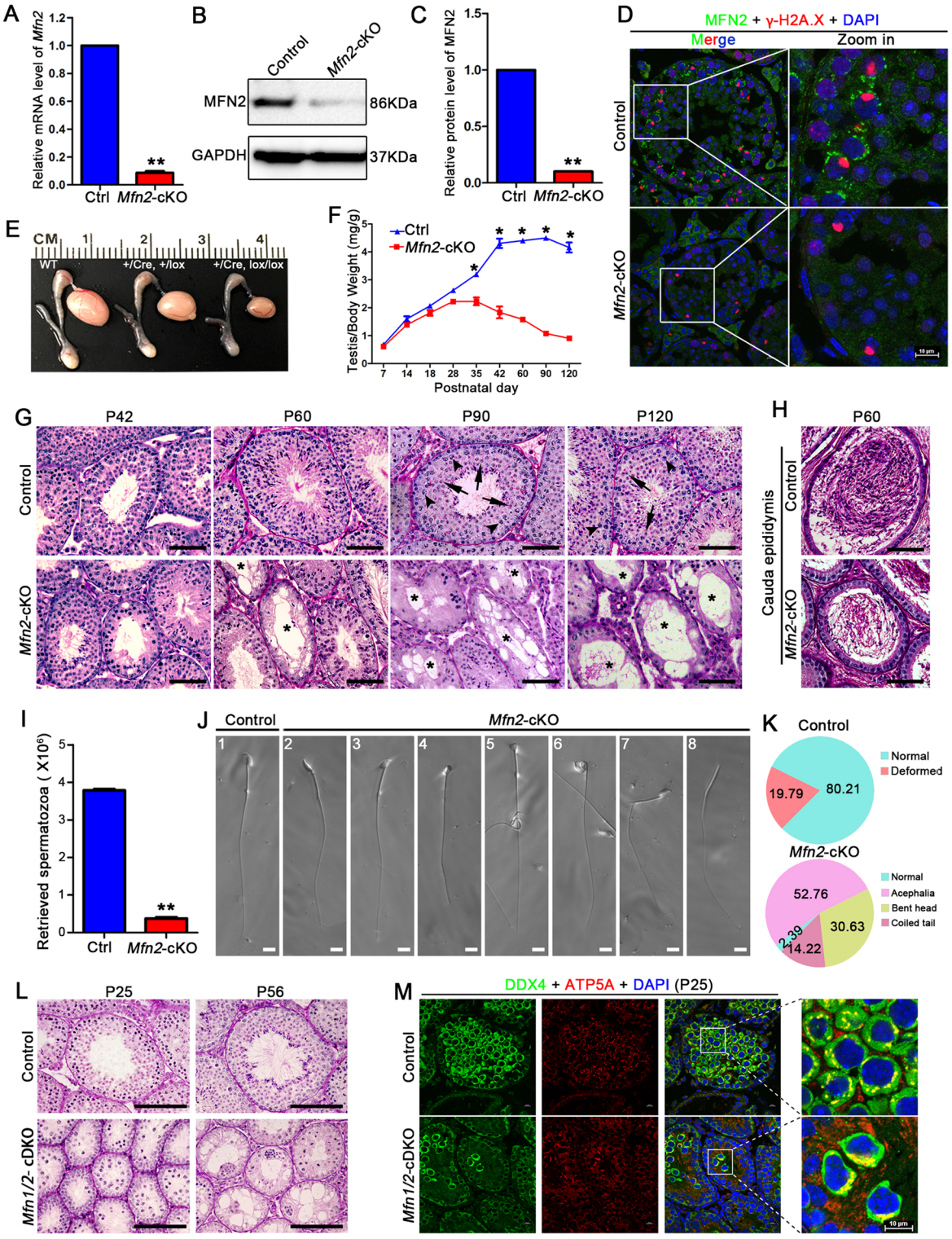

Fig. 2. Conditional ablation of MFN2 in postnatal male germ cells results in male infertility. (A-C) The mRNA and protein levels of *Mfn2* were detected in control and *Mfn2*-cKO testes using RT-qPCR (A) and western blots (B,C). Data are mean±s.e.m., n=5. **P<0.01 (two-tailed Student's t-test). GAPDH serves as a loading control. (D) Immunostaining showing that MFN2 was undetectable in the *Mfn2*-cKO testis sections. (E) Gross morphology of the testis and the epididymis from WT, heterozygote (Cre/+, $Mfn2^{+/flox}$) and *Mfn2*-cKO (Cre/+, $Mfn2^{flox/Del}$) mice at P56. (F) Testis growth curve shows that the *Mfn2*-cKO testis weight was significantly decreased from P35. Data are mean±s.e.m., n=5. *P<0.05 (two-tailed Student's t-test). (G,H) Histological analyses of testes (G) and cauda epididymides (H) from control and *Mfn2*-cKO mice at different ages are shown. Asterisk represents the vacuolated seminiferous tubules. Arrows indicate round spermatids. Arrowheads indicate pachytene spermatocytes. (I) Histograms showing the number of retrieved sperm from the control and *Mfn2*-cKO cauda epididymides. Data are mean±s.e.m., n=3. *P<0.01 (two-tailed Student's t-test) (J) Deformed sperm are shown in *Mfn2*-cKO mice. (K) Pie charts showing the proportional distribution of normal and malformed sperm in control and *Mfn2*-KO mice. (L) Histological analyses of testis sections from control and *Mfn1*/2-cDKO mice at P25 and P56. (M) Co-immunostaining of DDX4 and ATP5A in testis sections from control and *Mfn1*/2-cDKO mice at P25. Scale bars: 10 µm (D,J,M); 50 µm (G,H); 100 µm (L).

Development (2021) 148, dev196295. doi:10.1242/dev.196295

mitofusin-deficient germ cells. Using transmission electron microscope (TEM) analysis, we observed that mitochondria exhibit swelling and fragmentation in germ cells from adult *Mfn2*-cKO or *Mfn1*-cKO mouse testes (Fig. 3A,B; Fig. S5A). The thickness of IMC increased significantly in *Mfn2*-cKO PS (Fig. 3A; P=0.024, two-tailed Student's t-test). We then focused on *Mfn2*-cKO RS to further detail the mitochondrial defects. The mitochondrial aspect ratios (AR; major axis/minor axis of mitochondria) were used to calculate the length of mitochondria in RS in control and *Mfn2*-cKO mice. Although the AR of all mitochondria was not significantly decreased in *Mfn2*-cKO RS (Fig. 3C), the AR distribution displayed an increased percentage of short mitochondria with AR≤1.5 compared with that of controls (Fig. 3D). These data suggest that developmental defects of male germ cells in both *Mfn1*- and *Mfn2*-cKO mice could be due to the fragmentation and mitochondrial swelling in germ cells.

Given that MFN2 supports structural and functional communication between the mitochondria and ER, we then investigated whether the deletion of *Mfn2* in postnatal male germ cells disrupts MAM and ER homeostasis. We observed that the distance between mitochondria and ER was increased by ∼16% in *Mfn2*-cKO spermatids compared with control spermatids. Similarly, the percentage of mitochondria-ER contacts was significantly reduced by nearly 50% in *Mfn2*-cKO testes compared with that of controls (Fig. 3E,F). In addition, the ER-mitochondria contact coefficient (ERMICC) (Naon et al., 2016) was also reduced by more than 30% in *Mfn2*-cKO testes compared with that of controls (Fig. 3G). Notably, the ER displayed tube-like cisternae structures in control spermatids, whereas it was fragmented in *Mfn2*-cKO spermatids (Fig. 3B), implying that the ER structure was disrupted upon MFN2 deletion. To further confirm these observations, calreticulin (a MAM and ER marker protein) immunostaining was employed to examine the MAM structure in P18 and P60 testes. Calreticulin displayed a diffused granular pattern in the cytoplasm of *Mfn2*-cKO spermatocytes at P18 instead of the continuous perinuclear localization exhibited in the controls (Fig. 3H). Moreover, in P60 testes, the calreticulin signals in *Mfn2*-cKO germ cells appeared to be reduced and displayed diffused granular distribution compared with that of controls (Fig. 3I). Of note, unlike the observation in *Mfn2*-cKO spermatocytes, calreticulin does not exhibit any diffused signal pattern in *Mfn1*-cKO spermatocytes (Fig. S5B). These data suggest that MFN2 but not MFN1 may function in the regulation of the formation of MAM and ER structures.

Dynamic mitochondrial fusion and fission are known processes that regulate mitochondrial DNA (mtDNA) stability and energy production (Palmer et al., 2011; Westermann, 2010). To examine each, we first determined mtDNA copy number in *Mfn1*-cKO and/or *Mfn2*-cKO adult testes by quantitative real-time PCR (qPCR). Unexpectedly, we found that the mtDNA copy number was increased significantly in both *Mfn1*-cKO and *Mfn2*-cKO adult testes (Fig. 3J), which is in contrast to previous reports showing that conditional single knockout of either *Mfn1* or *Mfn2* in skeletal muscle did not alter mtDNA copy number (Chen et al., 2010). This difference implies that an additional MFN1/2 mechanism regulates mtDNA stability. We directly stained cytochrome c oxidase (COX, complex IV) and succinate dehydrogenase (SDH, complex II) activity to assess whether the function of respiratory complexes was affected by MFN1- or MFN2 deficiency. In line with the increased mtDNA copy number, COX activity increased in both *Mfn1*-cKO and *Mfn2*-cKO testis sections, whereas the SDH activity was unaltered (Fig. 3K). These results suggest that MFN1/2 deficiency in male germ cells leads to increased mitochondrial fission and mitochondrial metabolism disorder.

MFN2 interacts with nuage-associated proteins and affects their expression and piRNA production in testes

As MFN2 displays a granular cytoplasmic localization in male germ cells (Fig. 1), we assumed that MFN2 is involved in mitochondria-associated germinal structure formation. To test this hypothesis, we selected four mitochondrial-associated germinal granule proteins (also known as nuage-associated proteins), MIWI, DDX4, TDRKH and GASZ, to perform Co-IP in the testis and an HEK293T cell line. We found that, in MFN2 antibody immunoprecipitants, MIWI, DDX4, GASZ and TDRKH were strongly detected in WT testes (Fig. 4A). Likewise, in MIWI, TDRKH, DDX4 and GASZ antibody immunoprecipitants, MFN2 was detected in testes (Fig. 4B-E). These results suggest that MFN2 interacts with MIWI, TDRKH, DDX4 and GASZ in testes. We also examined their interaction in the cell line. When the full length of MFN2 was ectopically co-expressed with MIWI, TDRKH and DDX4 in HEK293T cells, MFN2 was pulled down by MIWI, TDRKH and DDX4, indicating the ability of MFN2 to interact with MIWI, TDRKH and DDX4 proteins (Fig. 4F,G). To validate the interaction specificity of MFN2 with these proteins, we chose hnRNPA2, a nuclear protein, which does not interact with MFN2 as a negative control. The result showed that Myc-hnRNPA2 could not interact with Flag-MFN2 in HEK293T cells (Fig. S5C).

Next, we examined whether the expression of MIWI, DDX4, GASZ and TDRKH was affected by the deletion of MFN2 in testes. Co-immunostaining revealed reduced levels of MIWI, DDX4 and GASZ in IMC and CB structures of *Mfn2*-cKO testes, whereas TDRKH displayed no apparent change (Fig. 4H; Fig. S5D-F). In *Mfn2*-cKO testes, both MIWI and DDX4 showed weaker staining in the IMC of PS and was barely detected in the CB of RS (Fig. 4H; Fig. S5D,E). GASZ also showed a decreased signal in both PS and RS within *Mfn2*-cKO testicular sections (Fig. 4H; Fig. S5F). As MFN1 was reported to interact with GASZ and is essential for spermatogenesis (Zhang et al., 2016), we also compared the expression and localization of DDX4, GASZ and TDRKH in *Mfn1*-cKO adult testes. However, unlike *Mfn2*-cKO testes, we found no obvious changes in expression or localization in *Mfn1*-cKO testes (Fig. S5G-I).

Nuage-associated proteins are documented in regulating piRNA biogenesis. This prompted us to determine whether MFN2 participates in the piRNA pathway. We chose P25 testes to examine the abundance and size distribution of piRNAs through small RNA-seq, as the morphology and the cell populations were comparable at P25 between WT and *Mfn2*-cKO testes. The results showed ∼50% decrease in the total piRNAs normalized to miRNA counts (Fig. 4I; Table S1), suggesting that MFN2 participates in piRNA biogenesis through its interaction with the nuage proteins. To investigate whether the abundance of piRNA precursors is affected by MFN2 deletion, we analyzed piRNA precursor levels in the *Mfn2*-cKO testis at P25. We found that the levels of piRNA precursors in *Mfn2*-cKO were comparable with those of WT (Fig. 4J). Next, we asked whether the retrotransposons were affected in *Mfn2*-cKO testes, because the nuage-associated proteins have been reported to repress retrotransposons to maintain genome integrity. We analyzed the levels of LINE1 and IAP mRNAs, and found that there were no significant changes between WT and *Mfn2*-cKO testes (Fig. 4K). Consistent with the level of LINE1 mRNA, the LINE1 ORF1 protein showed no activation in P60 *Mfn2*-cKO testes (Fig. 4L). Taken together, these results indicate that MFN2 interacts with nuage-associated proteins and participates in piRNA

Development (2021) 148, dev196295. doi:10.1242/dev.196295

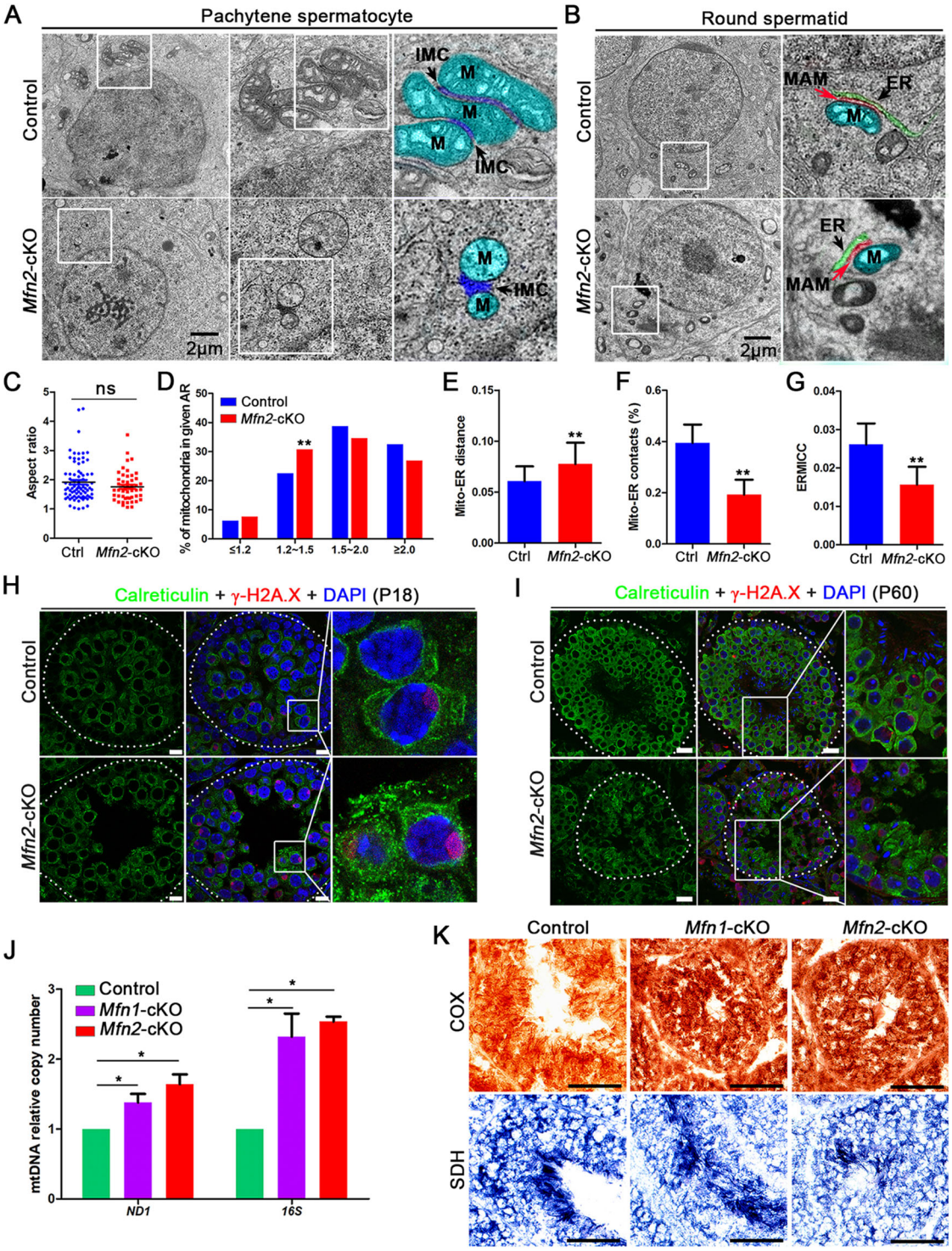

Fig. 3. MFN2 deficiency in postnatal germ cells causes mitochondria, ER and MAM defects. (A,B) Transmission electron microscope analyses of pachytene spermatocytes (PS; A) and round spermatids (RS; B) from *Mfn2*-cKO mouse testes at P60 are shown. Right panels show magnification of the boxed areas in the left panels. (C) Scatter plot showing the aspect ratio (AR) in RS from control and *Mfn2*-cKO mouse testes. AR represents the ratio of the major axis to the minor axis of mitochondria. (D) The distribution of AR in C showing an increased percentage of short mitochondria in *Mfn2*-cKO RS. ***P*<0.01 (two-tailed Student's *t*-test). (E,F) Histograms showing the distance (E) and contacts (F) between mitochondria and ER in RS from control and *Mfn2*-cKO mouse testes. **P*<0.05, ***P*<0.01 (two-tailed Student's *t*-test). (G) Histogram showing the ERMICC [mitochondrial-ER interface length/(mitochondrial perimeter×mitochondrial-ER distance)] values in RS from control and *Mfn2*-cKO mouse testes. Data are mean±s.e.m., *n*=3. ***P*<0.01 (two-tailed Student's *t*-test). (H,I) Co-immunostaining of calreticulin and γ-H2A.X in testis sections from control and *Mfn2*-cKO mice at P18 (H) and P60 (I). Nuclei were stained with DAPI. Dotted line indicates the outline of the seminiferous tubule. Right panels show magnification of the boxed areas in the left panels. (J) RT-qPCR analyses showing the mtDNA copy numbers in control, *Mfn1*-cKO and *Mfn2*-cKO mouse testes at P60. ND1 and 16S are the two genes encoded by mtDNA. Data are mean ±s.e.m., *n*=6. **P*<0.05 (two-tailed Student's *t*-test). (K) Respiratory enzymes COX (encoded by mtDNA) and SDH (encoded by nuclear DNA) staining of testis sections from adult control, *Mfn1*-cKO and *Mfn2*-cKO mice are shown. ER, endoplasmic reticulum; IMC, inter-mitochondrial cement; M, mitochondria; MAM, mitochondria-associated ER membranes. Scale bars: 2 μm (A,B); 20 μm (H,I); 50 μm (K).

Development (2021) 148, dev196295. doi:10.1242/dev.196295

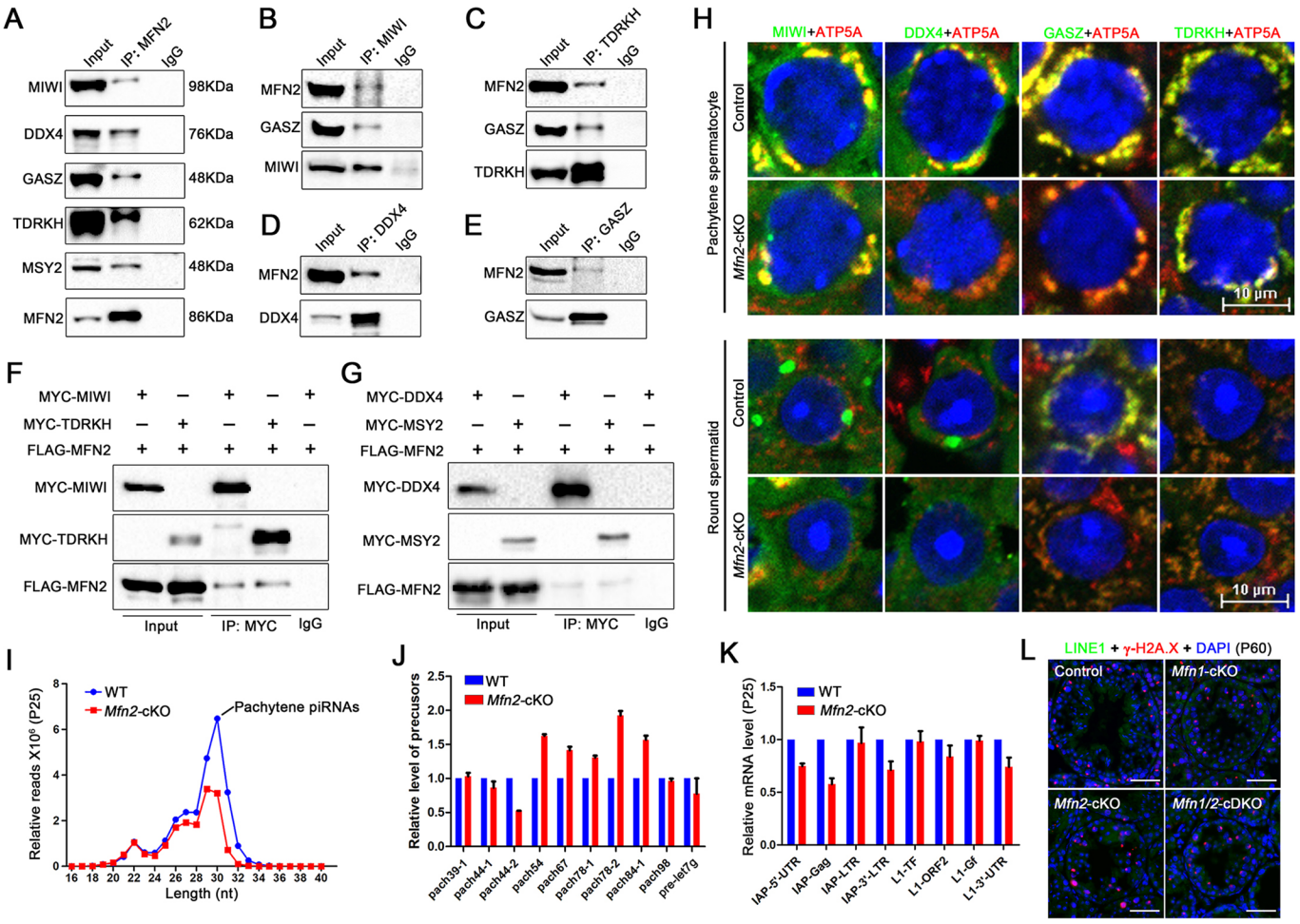

Fig. 4. MFN2 interacts with nuage-associated proteins and regulates their expressions in spermatogenic cells. (A) Co-immunoprecipitation of MFN2 followed by western blot detection of MIWI, DDX4, GASZ, TDRKH and MSY2 in adult mouse testes. (B-E) Reciprocal immunoprecipitation showing that MFN2 was detected in the immunoprecipitants from MIWI (B), TDRKH (C), DDX4 (D) and GASZ (E) in adult mouse testes. (F,G) MFN2 interacts with MIWI (F), TDRKH (F), DDX4 (G) and MSY2 (G) *in vitro*. HEK293T cells were transfected with indicated plasmids. After 48 h of transfection, immunoprecipitation was performed using anti-MYC antibodies and detected by anti-MYC and anti-FLAG antibodies. (H) Co-immunostaining of ATP5A with MIWI, DDX4, GASZ and TDRKH in pachytene spermatocytes and round spermatids from control and *Mfn2*-cKO mouse testes. (I) Size distribution of small RNA libraries from adult WT and *Mfn2*-cKO testes at P25. Data were normalized by microRNA reads (21-23 nt). (J,K) RT-qPCR analyses of indicated piRNA precursors (J) and different types of retrotransposon (K) in WT and *Mfn2*-cKO testes. miRNA precursor pre-let7g served as a control. Data are mean±s.e.m., n=6. (L) Co-immunostaining of LINE1 with γ-H2A.X in seminiferous tubules from adult control, *Mfn1*-cKO, *Mfn2*-cKO and *Mfn1*/2-cDKO mice. Scale bars: 10 μm (H); 50 μm (L).

pathways during spermatogenesis, but does not seem to directly participate in retrotransposon silencing.

RNA-seq revealed differentially expressed genes involved in mRNA processing in spermatogenic cells

To investigate the molecular consequences of the loss of MFN2 in spermatogenic cells, we compared the transcriptomes of purified PS and RS from WT and *Mfn2*-cKO adult testes using RNA-seq. Hierarchical clustering of differentially expressed genes (DEG) showed that, in PS, a total of 4046 genes were upregulated and 5324 genes were downregulated in *Mfn2*-cKO mice compared with WT mice. In RS, a total of 3756 genes were upregulated and 3186 genes were downregulated in *Mfn2*-cKO mice compared with WT mice (Fig. 5A,B; Fig. S6A,B; Tables S2,S3). To validate the RNA-seq data, we randomly selected the genes associated with ribosome transport (*Uba52*, *Rps20*, *Rpl21*, *Fau* and *Rpl26*), spliceosome and mRNA transport (*Pabpc1*, *Hspa2*, *Sf3b4*, *Acin1*, *Ncbp1* and *Nup188*) pathways for RT-qPCR analyses. The expression of genes related to ribosome transport pathways was increased more than twofold (except *Rps20*) in both *Mfn2*-cKO PS and RS compared with controls, in accord with the fold-changes determined by RNA-seq. Moreover, the expression of genes related to spliceosome and mRNA transport pathways were reduced by more than 50% in both *Mfn2*-cKO PS and RS (Fig. S6C,D). Taken together, these RNA-seq analyses suggest that MFN2 deficiency in testes influences the expression of genes that control multiple biological processes, including mRNA processing.

As shown above (Fig. 4I), we observed a ∼50% reduction of piRNA populations in *Mfn2*-cKO testes. Next, we asked whether the decreased level of piRNAs dysregulate transcripts in *Mfn2*-cKO PS and RS. As the function of piRNAs in regulating mRNA stability and directed meiotic transcript cleavage require the slicer activity of MIWI, a nuage-associated protein (Goh et al., 2015; Zhang et al., 2015), we compared the RNA-seq dataset of *Mfn2*-cKO with the published RNA-seq dataset of *Miwi*-KO (GEO accession number GSE64138) (Goh et al., 2015), including PS and RS. First, we compared the upregulated genes identified from *Mfn2*-cKO PS and RS with the 330 putative piRNA-targeting mRNAs reported by Goh et al. (2015). We found that ∼10% (34/330 in PS and 32/330 in RS)

Development (2021) 148, dev196295. doi:10.1242/dev.196295

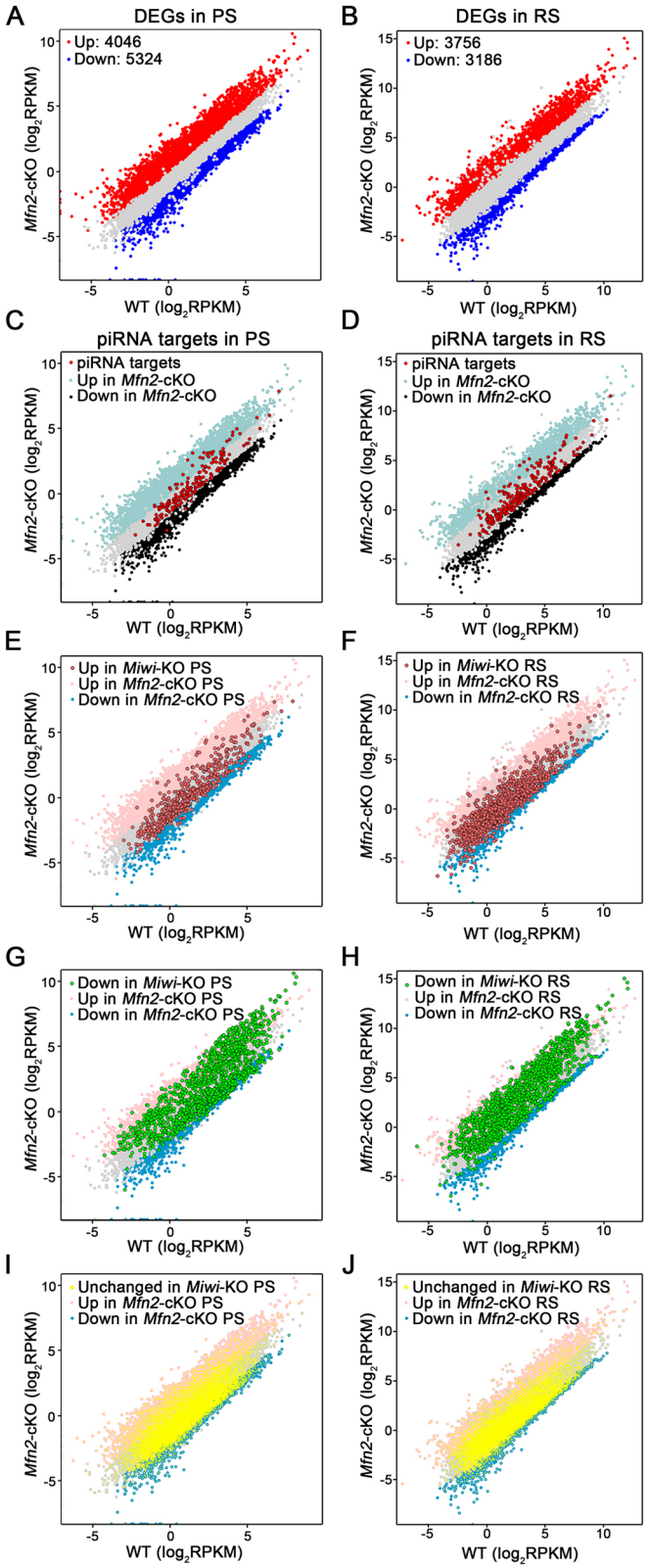

Fig. 5. Global gene expression is altered in *Mfn2*-cKO spermatogenic cells. (A,B) Scatter plots showing the differentially expressed genes in purified PS (A) and RS (B) from WT and *Mfn2*-cKO testes. Significantly regulated genes have a *P*-value of <0.05 and a fold change of >2.0. Two biological replicates are indicated in the plots. (C,D) Scatter plots showing the RNA-seq values sequenced from 330 piRNA-targeting genes in *Mfn2*-cKO versus WT PS (C) and RS (D). Each dot represents the average Log_2RPKM of an individual gene from different categories. (E-J) Scatter plots showing the upregulated genes in *Miwi*-KO PS (E) and RS (F), the downregulated genes in *Miwi*-KO PS (G) and RS (H), and the unchanged genes in *Miwi*-KO PS (I) and RS (J) mapped onto *Mfn2*-cKO RNA-seq dataset. RPKM, reads per kilobase per million mapped reads.

of piRNA-targeting mRNAs were upregulated in *Mfn2*-cKO spermatogenic cells (Fig. 5C,D; Tables S4,S5). With fewer piRNA-targeting mRNAs overlapped than expected (representation factor=0.9 and 0.8, respectively), the probability of this overlap is non-significant, with *P*-values of 0.077 (PS) and 0.230 (RS). When compared with the results from Goh et al. (2015), ∼20% (72/330) piRNA-targeting mRNAs were reported to be upregulated in *Miwi*-KO RS (Goh et al., 2015). Interestingly, only three transcripts overlapped between 32 upregulated piRNA-targeting mRNAs in *Mfn2*-cKO RS and 72 upregulated piRNA-targeting mRNAs in *Miwi*-KO RS (Table S5), likely reflecting the complexity of MFN2 in regulating spermatogenesis, which is distinct from MIWI. These analyses suggest that the 50% decrease of piRNA observed in *Mfn2*-cKO could influence the expression of ∼10% piRNA-targeting mRNAs. Second, we compared the overlapped dysregulated genes between *Mfn2*-cKO and *Miwi*-KO spermatogenic cells, including PS and RS. We took the *Mfn2*-cKO versus WT to scatter plots and mapped the genes upregulated in *Miwi*-KO PS (Fig. 5E) and RS (Fig. 5F), downregulated in *Miwi*-KO PS (Fig. 5G) and RS (Fig. 5H), and unchanged in *Miwi*-KO (Fig. 5I,J). The results showed that 74 genes are co-upregulated in both *Mfn2*-cKO and *Miwi*-KO PS (Fig. 5E; Fig. S7A), and 152 genes are co-upregulated in both *Mfn2*-cKO and *Miwi*-KO RS (Fig. 5F; Fig. S7B). This overlap of ∼10% (74/680, representation factor=0.8, *P*=0.049) and ∼7% (152/1971, representation factor=0.7, *P*=1.137e-7) upregulated genes, respectively, is significantly less than was expected. As such, these overlapping upregulated genes in PS and RS of *Mfn2*-cKO and *Miwi*-KO were only a small portion of the two gene sets, which indicates that they are unlikely to be co-regulated by MIWI and MFN2 in testes.

Furthermore, 304 and 108 genes were found to be commonly downregulated in *Mfn2*-cKO and *Miwi*-KO PS (Fig. 5G; Fig. S7C) and RS (Fig. 5H; Fig. S7D), respectively, which accounts for ∼25% (304/1541, representation factor=1.1, *P*=0.004) and ∼6% (108/1757, representation factor=0.7, *P*=1.846e-7) of downregulated genes in *Miwi*-KO PS and RS, respectively. Interestingly, the 304 overlapping genes identified in PS was significantly more than expected, whereas the 108 overlapping genes in RS was significantly less than expected, indicating that the 304 overlapping downregulated genes in PS are related, whereas those overlapping downregulated genes in RS are not. Moreover, the 304 downregulated genes in PS overlaps are mostly related to germ cell development, spermatogenesis and meiotic division (Fig. S7E,F). Together, MFN2 and MIWI (a nuage protein) only regulate a smaller overlapping subset of RNAs than expected, suggesting that although MFN2 and MIWI are bound in testes, they regulate mostly non-overlapping sets of mRNAs.

MFN2 associates with polysomes and interacts with translational regulator MSY2

Because some of the MFN2 interaction proteins, like MIWI and DDX4, are associated with RNA processing and translational machinery in spermatogenesis (Grivna et al., 2006; Nagamori et al., 2011), we wanted to determine whether MFN2 plays a role in mRNA translation. To test this relationship, we first subjected adult testicular extracts to sucrose density polysome gradients. MFN2 co-sedimented with both the monosome (80S) and polysome fractions (Fig. 6A). Similar to RPS6, the addition of EDTA to dissociate the large and

Development (2021) 148, dev196295. doi:10.1242/dev.196295

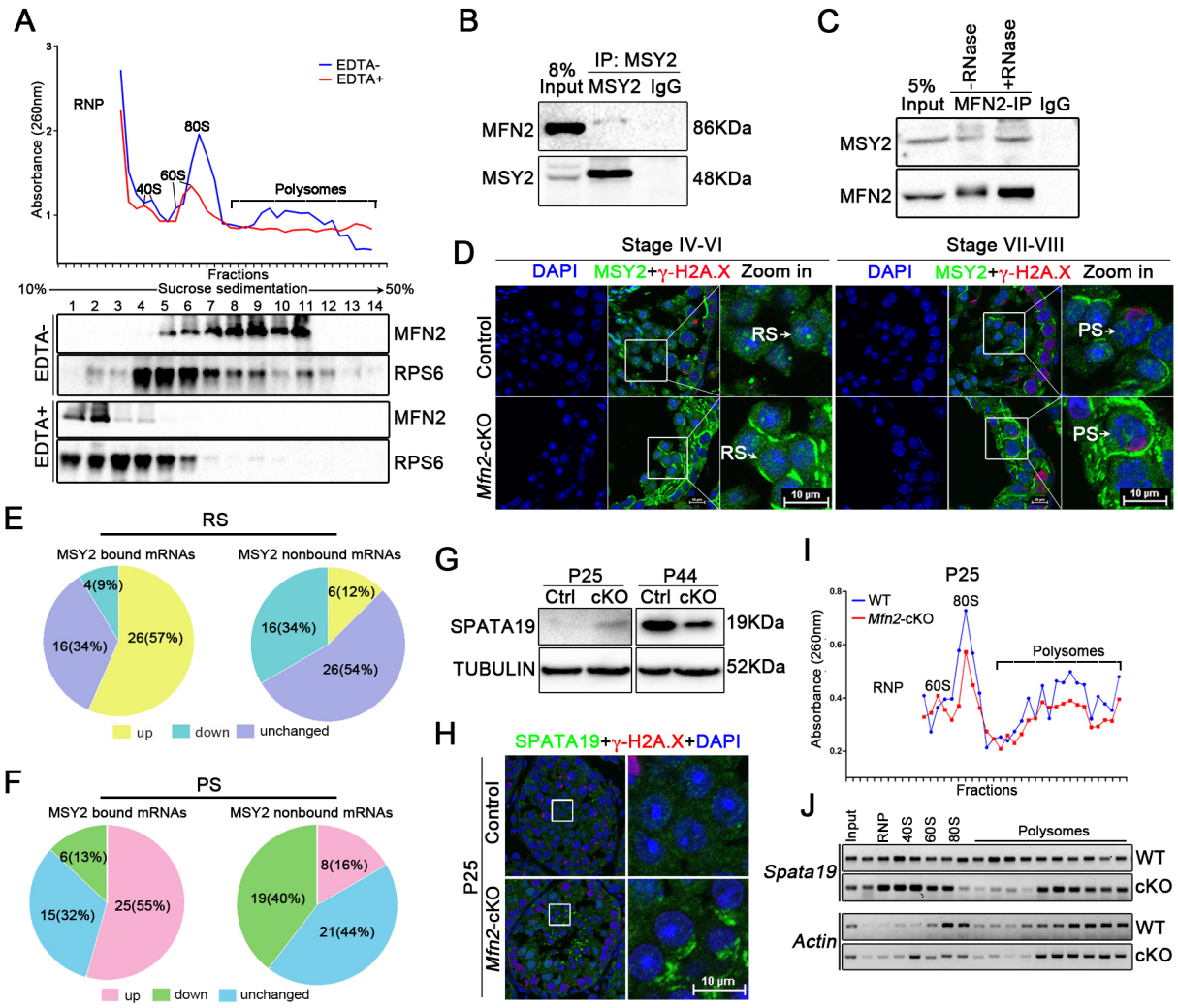

Fig. 6. MFN2 is associated with polysomes and regulates the fate of gamete-specific mRNAs. (A) EDTA-untreated (EDTA–) and -treated (EDTA+) post-nuclear testicular extracts from adult WT mice were fractionated on linear 10-50% sucrose density gradients and analyzed by UV spectrometry (top). The distribution of MFN2 protein is detected by western blotting (bottom). RPS6 protein serves as a positive control. (B,C) Reciprocal immunoprecipitation showing that MFN2 interacts with MSY2 in an RNase-independent manner. (D) Co-immunostaining of MSY2 and γ-H2A.X in stage IV-VI and VII-VIII seminiferous tubules from adult control and *Mfn2*-cKO testes. (E,F) Pie charts showing the ratio of differentially expressed MSY2-bound and non-bound gamete-specific mRNAs in RS (E) and PS (F) from the *Mfn2*-cKO RNA-seq dataset. (G) Western blot analysis of the protein levels of SPATA19 in control and *Mfn2*-cKO testes at P25 and P44. (H) Co-immunostaining of SPATA19 and γ-H2A.X in P25 testes from control and *Mfn2*-cKO mice. (I) Cytoplasmic polysome profiling of control (blue) and *Mfn2*-cKO (red) testes at P25. (J) Distribution of *Spata19* and *Actb* mRNAs across the density gradients from I, determined by semi-quantitative RT-PCR. Scale bars: 10 μm.

small ribosomal subunits shifted MFN2 to the ribonucleoprotein (RNP) fractions of the gradients. These data suggest that MFN2 associates with cytoplasmic monosomes and polysomes.

Given that MSY2 was exclusively enriched in both the meiotic and post-meiotic germ cells (Gu et al., 1998), and has been reported to participate in both transcription and mRNA translation (Yang et al., 2005b), we next asked whether MFN2 complexes with MSY2 to regulate mRNA translation in testes. We found that MFN2 and MSY2 could reciprocally pull down each other independent of RNA, indicating a direct interaction between these two proteins *in vivo* (Fig. 6B,C). Because our unbiased RNA-seq data showed an increased level of *Msy2* mRNA in both *Mfn2*-cKO PS and RS, we then examined the protein level of MSY2 in adult control and *Mfn2*-cKO testes by immunofluorescence. In control testes, MSY2 was broadly expressed in nearly all types of spermatogenic cells and showed a disperse distribution in the cytoplasm and nucleus in PS and RS (Fig. 6D). However, in *Mfn2*-cKO testes, the cytoplasmic MSY2 increased in PS and RS, and the MSY2 foci within the RS nucleus had almost disappeared (Fig. 6D). Considering that MSY2 marks specific mRNAs in the nucleus for cytoplasmic storage and links transcription and mRNA storage/translational delay in meiotic and post-meiotic male germ cells (Yang et al., 2005a), we analyzed the transcript levels of MSY2-bound and -unbound mRNAs in our RNA-seq data. Intriguingly, for MSY2-bound gamete-specific mRNAs, of which ∼57% (26/46) is upregulated in *Mfn2*-cKO RS, including *Msy2* itself, ∼9% (4/46) downregulated and the remaining 34% (16/46) mRNAs are unaffected (Fig. 6E; Fig. S8A; Table S6). In contrast, MSY2-unbound mRNAs in *Mfn2*-cKO RS were either downregulated (34%, 16/48) or unaffected (54%, 26/48), and only 12% of MSY2-unbound mRNA was upregulated (6/48) (Fig. 6E; Fig. S8B; Table S7). The situation in *Mfn2*-cKO PS is almost the same as in RS (Fig. 6F; Tables S8,S9). These results indicate that MFN2 interacts with cytoplasmic MSY2 in spermatogenic cells to regulate the fates of MSY2-bound gamete-specific mRNAs.

Development (2021) 148, dev196295. doi:10.1242/dev.196295

To further explore the role of MFN2 during translation, we assessed whether any proteins were mistranslated from the MSY2-bound gamete-specific mRNAs. As SPATA19 is a mitochondrial protein previously reported to be expressed in haploid spermatids in P28 testes (Doiguchi et al., 2002; Matsuoka et al., 2004) and germ cell-specific *Spata19* knockout mice displayed male sterility (Mi et al., 2015), we chose to examine SPATA19 at the protein level in P25 testes from control and *Mfn2*-cKO mice. Notably, we found that the SPATA19 protein could be detected in P25 *Mfn2*-cKO testes, whereas it was not detected in control testes (Fig. 6G,H). To determine whether the early-translated SPATA19 protein observed in *Mfn2*-cKO testes is caused by translational activity, we measured cytoplasmic translation by quantifying the polysome distribution of *Spata19* mRNAs, with β-actin (*Actb*) as an internal control in WT and *Mfn2*-cKO testes at P25. The distribution of *Spata19* mRNA shifted toward the heavier polysome fractions, whereas the distribution of *Actb* mRNA showed no apparent change (Fig. 6I,J), indicating increased SPATA19 translational activity in the cytoplasm of *Mfn2*-cKO testicular cells. Taken together, these results indicate that MFN2 is associated with polysomes and interacts with MSY2 (non-nuage protein) to control the fates of MSY2-bound gamete-specific mRNAs (e.g. *Spata19*) during spermatogenesis.

DISCUSSION

Although two recent studies have reported that both MFN1 and MFN2 play essential functions in spermatogonial differentiation and meiosis through a dynamic mitofusin-mediated mitochondrial and ER stress mechanism in spermatogenesis (Chen et al., 2020; Varuzhanyan et al., 2019), its roles in post-meiotic spermatogenic cell development have remained elusive. In this study, we showed that loss-of-function of either MFN1 or MFN2 in postnatal male germ cells results in male sterility in mice and, more importantly, we revealed a previously unknown role of MFN2 upon interaction with nuage-proteins and MSY2 that controls the fate of many spermatogenic cell mRNAs. These findings uncovered a novel role of MFN2 in late spermatogenesis and added another layer of MFN1/2 molecular functions onto post-meiotic male germ cell development. Interestingly, we found that the *Mfn2*-cKO mouse phenotype is age-dependent, with germ cells beginning their decline after P35. In comparison, *Mfn1*-cKO mice showed a severe phenotype with an observation of seminiferous tubule vacuolization as early as P28. Similarly, *Vasa*-Cre-mediated *Mfn1* or *Mfn2* single knockout mice (*Vasa*-Cre; *Mfn1*$^{flox/flox}$ or *Vasa*-Cre; *Mfn2*$^{flox/flox}$) were also infertile and displayed a distinct meiotic arrest phenotype, with a relative earlier blockage of meiosis in *Mfn1*-cKO than in *Mfn2*-cKO mice (Chen et al., 2020). The discrepancy of phenotypes between this study and the previous study possibly reflects the differences in Cre recombinase expression, as *Vasa*-Cre appears much earlier than *Stra8*-Cre in the male germline. Thus, the phenotypic differences between *Mfn1*- and *Mfn2*-cKO mice mediated by either *Stra8*-Cre or *Vasa*-Cre suggest that MFN1 plays a distinct role from MFN2, not only in regulating spermatogonial differentiation but in promoting meiotic and post-meiotic spermatogenic cell development. Notably, consistent with previous reports (Varuzhanyan et al., 2019), the *Stra8*-Cre induced *Mfn1/2* double knockout mice presented a defective meiosis phenotype of the near loss of PS, suggesting that MFN1 cooperates with MFN2 to regulate spermatogonial differentiation and meiosis. However, based on transgene rescue experiments (Chen et al., 2020), it does not appear to be likely that MFN1 mutually compensates with MFN2 in male germ cell development. This is consistent with the view that the regulation of spermatogenesis by these two mitochondrial fusion proteins at different stages is independent of other currently unknown functions beyond the mitochondrial fusion mechanism. The identity of the distinct underlying molecular mechanism between MFN1 and MFN2 in regulating male germ cell development needs further investigation.

Several MFN2 interactive proteins identified in this work, including MIWI, DDX4, GASZ and TDRKH, were also present in the MAM fractions in our previous mass spectroscopy data (Wang et al., 2018). Remarkably, the proteins identified located in MAMs are possibly responsible for regulating piRNA biogenesis and mRNA translation as they are a feature of nuage-associated proteins in germ cells. The fact that we observed reduced pachytene piRNA production in *Mfn2*-cKO testes suggests that mitofusins might have a function in piRNA biogenesis. We observed an ∼50% reduction in *Mfn2*-cKO pachytene piRNA, which may explain, to a lesser extent, the elevated mRNA levels in *Mfn2*-cKO PS and RS determined by RNA-seq, because pachytene piRNA could target meiotic mRNA cleavage (Goh et al., 2015). Surprisingly, the transposable elements (TEs) were not activated despite the decrease in pachytene piRNA in *Mfn2*-cKO testes. These data are in agreement with a previous report, which showed that the activity of TEs was not perturbed in *Vasa*-Cre-mediated *Mfn2* conditional knockout mice (Chen et al., 2020). The possible reason for this is that the reduced piRNAs in *Mfn2*-cKO are mostly not associated with TEs or repeats (NRapiRNAs) (Larriba and Del Mazo, 2018). However, we could not exclude the possibility of reduced piRNA biosynthesis in this study as an indirect effect caused by a decrease of piRNA biogenesis proteins, such as MIWI, DDX4, GASZ, etc. in *Mfn2*-cKO testes.

Interestingly, our data reveal that both MIWI and DDX4 are absent in the CB of *Mfn2*-cKO RS, resembling MIWI absence in the CB of *Tdrkh*-cKO spermatids (Ding et al., 2019). Unlike the reduced MIWI and GASZ expression, TDRKH expression was not affected in *Mfn2*-cKO spermatogenic cells, even though TDRKH was identified as interacting with MFN2. TDRKH expression was also unchanged in the *Miwi*-KO mice (Ding et al., 2019). The observations can be reconciled given that TDRKH is instrumental in binding to mitochondria to recruit MIWI to IMC and CB. These are the two typical nuage structures localized at spermatocytes and spermatids, respectively. Given the feature that TDRKH is a mitochondrial membrane-anchored protein, and MFN2 is a mitochondrial fusion protein (Hales and Fuller, 1997; Saxe et al., 2013), it has raised the possibility that the recruitment function of TDRKH requires the coordinated regulation of MFN2.

MFN2 is enriched in monosome and polysome fractions in spermatogenic cells and interacts with MSY2 to mediate MSY2-bound gamete-specific mRNA fates. MSY2 showed increased cytosolic expression in both PS and RS upon MFN2 depletion. This discovery raises the possibility that MFN2 partners with MSY2-bound mRNA for its function, because MSY2 was enriched in the RNP fraction and regulates mRNA stability, storage and translation delay in spermatogenesis (Yang et al., 2005a). Interestingly, MFN2 is not a known transcription factor, chromatin regulator or predicted RNA-binding protein. The global changes in the transcriptome of *Mfn2*-cKO spermatogenic cells might be indirectly caused by decreased piRNA abundance and misregulation of MSY2. The ∼50% decrease of piRNA might dysregulate a portion of meiotic transcripts, for example the piRNA-targeting transcripts. Besides, most of the interaction proteins of MFN2 are associated with RNA processing and the perturbation of the interaction protein could alter RNA transcript levels. Many MSY2-bound mRNAs are gamete-specific transcripts that are usually expressed in meiotic and post-meiotic cells. They should be subject to translational delay when

Development (2021) 148, dev196295. doi:10.1242/dev.196295

they are stored in the germ cell cytoplasm (Yang et al., 2007). MSY2 is known to repress translation of and prevent degradation of target RNAs (Xu and Hecht, 2008; Yang et al., 2005a). In the present study, if MFN2, acting as a partner protein, is required for both of those functions, we would expect that MSY2 target RNA levels would decrease in the *Mfn2*-cKO, even in the presence of increased MSY2. In contrast, though, we observed that 57% of the MSY2-bound RNAs showed higher expression in the *Mfn2*-cKO (versus 12% of MSY2-unbound RNAs). At the same time, the SPATA19 protein (encoded by MSY2 target RNA) was expressed prematurely at P25 in the *Mfn2*-cKO. One possible explanation is that absence of MFN2 compromises the translational repression by MSY2 but does not disturb its ability to protect target RNAs from degradation. Thus, increased MSY2 in the *Mfn2*-cKO may be more efficient at keeping the target RNAs safe, but without MFN2 it would not prevent their ectopic translation. However, further experiments are needed to elucidate the effects of MFN2 on the expression of MSY2 binding/nonbinding mRNAs during germ cell development. Specifically, it will be important to determine whether other MSY2 targets besides SPATA19 are expressed early in the *Mfn2*-cKO testes.

In conclusion, we report a novel role of MFN2 in controlling mRNA fates during spermatogenesis through interactions with both nuage-associated proteins and translation regulator MSY2. We propose that MFN2 associates with several mRNA translation-associated proteins such as MSY2, MIWI and DDX4 at the cytoplasmic nuage and/or MAM, and it likely serves as a scaffold to recruit mRNA, polysomes and other RNA binding proteins in both PS and RS to control gamete-specific transcript delay during spermatogenesis (Fig. S8C,D). This finding extends beyond the known functions of MFN2 in regulating mitochondrial fusion processes and spermatogenesis.

MATERIALS AND METHODS

Animals and ethics statement

All animal procedures were approved by the Institutional Animal Care and Use Committee (IACUC) of Tongji Medical College, Huazhong University of Science and Technology, China, and the mice housed in the specific pathogen-free facility of Huazhong University of Science and Technology. All experiments with mice were conducted ethically according to the Guide for the Care and Use of Laboratory Animal guidelines. Floxed *Mfn1* or *Mfn2* mice were previously created (Chen et al., 2007). The mice harboring the floxed *Mfn1* or *Mfn2* allele purchased from the Jackson Laboratory (stock no. 026401 and 026525). *Mfn1*$^{flox/flox}$ and/or *Mfn2*$^{flox/flox}$ female mice were crossed with *Stra8*-Cre male mice (Jackson Laboratory, stock no. 008208) to obtain *Stra8*-Cre; *Mfn1*$^{+/flox}$ and/or *Mfn2*$^{+/flox}$ males, then the *Stra8*-Cre; *Mfn1*$^{+/flox}$ and/or *Mfn2*$^{+/flox}$ male mice were further bred with *Mfn1*$^{flox/flox}$ and/or *Mfn2*$^{flox/flox}$ to obtain *Stra8*-Cre; *Mfn1*$^{flox/del}$ and/or *Mfn2*$^{flox/del}$ (designated as *Mfn1*-cKO and *Mfn2*-cKO) males.

Antibodies

The details of all commercial antibodies used in this study are presented in Table S10.

Histological analysis, immunostaining and imaging

Testes and epididymides from control and cKO mice were collected and fixed in Bouin's solution (Sigma-Aldrich, HT10132) at 4°C overnight and then washed with 75% alcohol five times for 30 min each time. Samples were then embedded in paraffin and 5 µm sections were cut using a ThermoFisher Scientific CryoStar NX50 cryostat and stained with periodic acid-Schiff (PAS) after being dewaxed and rehydrated. Slides were then mounted with Permount (Fisher Chemical™ SP15-100) and imaged using a ZEISS microscope. For immunofluorescence staining, testes were fixed in 4% paraformaldehyde (PFA) in PBS overnight at 4°C and embedded in Tissue-Tek optimal cutting temperature (OCT) compound (Sakura Finetek, 4583) on dry ice. A 5 µm thick section was cut and microwaved in 0.01 M sodium citrate buffer (pH 6.0) for 5 min to retrieve antigen. After rinsing with PBS three times, the sections were blocked in blocking solution (containing 3% normal goat serum and 3% fetal bovine serum in 1% bovine serum albumin) for 1 h at room temperature (RT). Testis sections were then incubated with primary antibodies (Table S10) diluted in blocking solution overnight at 4°C. After washing with PBS, sections were incubated with Alexa Fluor 488 goat anti-rabbit IgG (1:500; A32731, Invitrogen) and/or Alexa Fluor 594 goat anti-mouse IgG (1:500, A11032, Invitrogen) for 1 h at RT and then stained with DAPI for 5 min, washed in PBS and mounted using 80% glycerol. Confocal fluorescence microscopy was conducted using a confocal A1 laser microscope (Nikon, A1 HD25).

TUNEL analyses

Testes were fixed in Bouin's solution, embedded in paraffin and sectioned (5 µm). TUNEL staining was performed using One Step TUNEL Apoptosis Assay Kit (Meilunbio, MA0223) according to the manufacturer's instructions. Images were obtained using a FluoView 1000 microscope (Olympus).

Transmission electron microscopy

Transmission electron microscopy was performed as previously described with some modifications (Wang et al., 2018). In brief, testes from control and cKO mice were fixed in 0.1 M cacodylate buffer (pH 7.4) containing 3% PFA and 3% glutaraldehyde plus 0.2% picric acid for 2 h at 4°C, then for 1 h at RT. After three washes with 0.1 M cacodylate buffer, the samples were post-fixed with 1% OsO4 for 1 h at RT. Then the samples were dehydrated in an ethanol series and embedded in an Eponate mixture (Electron Microscopy Sciences) for polymerization for 24 h at 60°C. Ultrathin sections (~70 nm) were cut using a diamond knife. The sections were re-stained with uranyl acetate and lead citrate and then photographed using a TEM (FEI Tecnai G2 12). For the calculation of the ERMICC contact index, the formula is: LIN/(PerM×DistER-M). LIN represents the interface length between mitochondria and ER; PerM indicates mitochondria perimeter; DistER-M is the distance between mitochondria and ER. Approximately 100 mitochondria were used to calculate for Mito-ER distance, Mito-ER contacts, and ERMICC contact index.

Cell culture and transfection

HEK293T (293T) cells were cultured in DMEM medium with 10% fetal bovine serum (Gibco, 10270106). Transfection was performed using Lipofectamine 2000 (Invitrogen) according to the manufacturer's instructions. For the transfection of the plasmid, 4 µg DNA was used in a 45 mm diameter plate.

Sertoli cell purification

For Sertoli cell isolation, testes from adult mice were dissected in DHANKS medium and incubated in DMEM/F12 medium containing 1 mg/ml collagenase IV, 0.5 mg/ml deoxyribonuclease I and 0.5 mg/ml hyaluronidase for 10 min at 37°C. After centrifugation (100 ***g***), the precipitates were collected and incubated in the DMEM/F12 medium with 2.5 mg/ml trypsin and 0.5 mg/ml deoxyribonuclease I for 10 min at 37°C. Then seminiferous tubules were incubated with DMEM/F12 containing 10% fetal bovine serum for 5 min to inhibit the trypsin digestion. Subsequently, Sertoli cells were collected after filtering through 40 µm pore-size nylon mesh and stored at −80°C for the experiments.

Protein extracts and western blots

Protein extracts were prepared from mouse tissues using RIPA lysis buffer [150 mM sodium chloride, 1.0% NP-40, 0.5% sodium deoxycholate, 0.1% SDS and 50 mM Tris (pH 8.0)]. Protein extracts were denatured with 2× loading buffer [4% SDS, 10% 2-mercaptoethanol, 20% glycerol, 0.004% bromophenol blue, 0.125 M Tris-HCl (pH 6.8)] at 95°C for 10 min and run on a 10% SDS-PAGE, followed by transfer to PVDF membrane. The membrane was probed with primary antibodies (Table S10) followed by secondary antibody treatment at 1:10,000 dilutions (anti-mouse HRP and anti-rabbit HRP, Abbkine, A25012 and A21020, respectively). Immun-Star™

Development (2021) 148, dev196295. doi:10.1242/dev.196295

HRP (1705040, Bio-Rad) was used for chemiluminescence detection, and was photographed using the ChemiDoc XRS+ system (Bio-Rad).

Co-immunoprecipitation

For *in vivo* Co-IP, mouse testes were homogenized in lysis buffer [20 mM HEPES (pH 7.3), 150 mM NaCl, 2.5 mM $MgCl_2$, 0.2% NP-40 and 1 mM DTT] with protease inhibitor cocktail (P1010, Beyotime). The relevant antibody and pre-cleaned magnetic protein A/G beads (blocking beads with bovine serum albumin 10% for 1 h to reduce the background before use) were added to the tissue lysate. RNaseA digestions were performed by adding RNase A (TransGen Biotech, GE101-01) at a final concentration of 500 µg/ml, followed by incubation for 3 h at 4 C followed by 30 min at RT. The lysate was incubated overnight at 4°C with gentle agitation to form the immunocomplex, and the magnetic beads were washed using the lysis buffer five times. The pellet was re-suspended with 40 µl elution buffer [1% SDS, 10 mM EDTA, 50 mM Tris (pH 8.0), 1× protease inhibitor] for 30 min at 70°C (with vortexing every 5-10 min). The eluate was transferred to a fresh tube, then 10 µl 5× SDS loading buffer was added, followed by boiling for 10 min. For *in vitro* Co-IP, full-length *Mfn2* complementary DNA (cDNA) was cloned into a modified pcDNA3 vector encoding a 2× FLAG-tag, and full-length *Miwi*, *Ddx4*, *Msy2* and *Tdrkh* cDNAs were cloned into a pCMV vector containing the N-terminal c-Myc epitope tag (Clontech Laboratories, K6003-1). HEK293T cells were transfected with indicated plasmids using Lipofectamine 2000 (Life Technologies). After 48 h, immunoprecipitation was performed using anti-MYC rabbit polyclonal antibody (4 µg antibody in 500 µl cell lysate, 10828-1-AP, Proteintech), followed by a western blot to identify protein interactions.

mtDNA copy number analysis

To quantify the amount of mtDNA present per nuclear genome, total DNA was extracted using the DNeasy Blood and Tissue Kit (Qiagen) and used for the detection of mtDNA copy number by quantitative real-time PCR (qPCR) using *Nd1*, 16S and *Hk2* primers (Table S11) and quantified using the $2^{-\Delta\Delta Ct}$ method.

COX/SDH staining enzyme histochemistry

COX and SDH activities were investigated separately using procedures modified from Ross (2011) and Jiang et al. (2017). Briefly, fresh testes tissues were quickly collected, rapidly frozen in liquid nitrogen, embedded in OCT compound, cryosectioned into 10-µm-thick sections, mounted on slides and left to air dry briefly. For COX staining, freshly prepared incubation buffer A (0.8 ml 5 mM 3,3′-diaminobenzidine tetrahydrochloride, 0.2 ml 500 mM cytochrome c, 10 ml catalase) was added to the slides. After incubation for 40 min at 37°C, slides were washed three times with 0.1 M PBS (pH 7.0) and dehydrated in an ethanol series (70%, 70%, 95%, 95%, 99.5%). Slides were then cleared with at least two changes of xylene and mounted with Permount Mounting Medium (Sinopharm, 10004160). For SDH staining, freshly prepared incubation buffer B [0.8 ml 1.875 mM nitroblue tetrazolium (NBT), 0.1 ml 1.3 M sodium succinate, 0.1 ml 2.0 mM phenazine methosulphate, 10 ml 100 mM sodium azide] was applied and incubated for 40 min at 37°C. Slides were washed in three changes of 0.1 M PBS, incubated with acetone solutions (30%, 60% and 90% in increasing then decreasing concentration) to remove unbound NBT, and mounted with an aqueous mounting medium for bright-field microscopy.

RNA isolation, reverse transcription and RT-qPCR

Total RNA was extracted from mouse tissues using Trizol reagent (Invitrogen, 15596-025) following the manufacturer's instructions. For cDNA synthesis, 1 µg of RNA was treated with DNase I (Promega, M6101) to remove the residual genomic DNA and reverse transcribed with cDNA Synthesis Kit (Thermo Fisher Scientific, 4368814). RT-qPCR was performed using an SYBR Premix on a StepOne Plus machine (Applied Biosystems, 4309155). Relative gene expression was analyzed using the $2^{-\Delta\Delta Ct}$ method with *Arbp* as an internal control. All primers are shown in Table S11.

Purification of spermatogenic cells

The STA-PUT method based on sedimentation velocity at unit gravity (Bellve, 1993; Bellve et al., 1977) was used to purify the PS and RS from adult WT and *Mfn2*-cKO mouse testes. We assessed cellular morphology using phase contrast microscopy to determine the purity of the cell population. PS and RS with ≥90% purity were used for RNA-seq analyses.

RNA sequencing and bioinformatics analysis

After purification of PS and RS from WT and *Mfn2*-cKO testes, total RNA was isolated using the Trizol reagent following the manufacturer's protocol and treated with DNase I to digest residual genomic RNA. The purity, concentration and integrity were assessed using a NanoDrop 2000 spectrophotometer (Thermo Fisher Scientific), a Qubit RNA Assay Kit in Qubit 2.0 Fluorometer (Life Technologies) and a Nano 6000 Assay Kit of the Bioanalyzer 2100 system (Agilent Technologies), respectively. Then, a total amount of 2 µg of RNA per sample was used to prepare poly(A+)-enriched cDNA libraries using the NEBNext Ultra RNA library Prep Kit for Illumina (New England Biolabs) according to the manufacturer's instructions, and base pairs (raw data) were generated by the Illumina Hi-Seq 2500 platform. Raw reads were processed with cutadapt v1.9.1 to remove adaptors and perform quality trimming. Trimmed reads were mapped to the UCSC mm10 assembly using HiSAT2 (V2.0.1) with default parameters. Differentially expressed genes for all pairwise comparisons were assessed by DESeq2 (v1.10.1) with internal normalization of reads to account for library size and RNA composition bias. Differentially regulated genes in the DESeq2 analysis were defined as twofold changes with an adjusted *P*-value of <0.05. Gene Ontology (GO) and Kyoto Encyclopedia of Genes and Genomes (KEGG) analyses were conducted using the database for annotation, visualization and integrated discovery (DAVID) (Dennis et al., 2003). The rich factor=number of DEGs in GO term/total number of genes in GO term. The larger the rich factor is, the higher enrichment is.

Small RNA-seq library preparation and sequencing

For preparing small RNA-seq libraries, two biological testis samples at P25 from WT and *Mfn2*-cKO mice were collected. Total RNAs were extracted using TRIzol reagent (Invitrogen) and subsequently processed to prepare small RNA-seq library and sequenced as previously described (Dong et al., 2019). For the length distribution of piRNA analysis, data were normalized by miRNA reads (21-23 nt) from small RNA-seq.

Sucrose density gradient fractionation and polysome profiling

Testicular seminiferous tubules were dissected and collected according to previous literature with minor modifications (Aboulhouda et al., 2017; Karamysheva et al., 2018). Briefly, after adding polysome extraction buffer [20 mM Tris-HCl (pH 7.4), 100 mM KCl, 5 mM $MgCl_2$, 1 mM DTT, 0.5% NP-40, 1× protease inhibitor cocktail (EDTA-free), 200 µg/ml CHX, 200 units/ml RNase inhibitor], the tubules were transferred to a small (0.5-1.0 ml) Dounce homogenizer to disrupt the tissues with seven to eight strokes of the glass pestle. The samples were centrifuged at 12,000 ***g*** at 4°C for 10 min to collect the supernatant into a new tube. Then, DNase I (final 5 U/ml) was added into the tube, and the tube was placed on ice for 30 min to allow the DNase I to degrade any DNA contamination. Equal amounts of cytoplasmic lysates were carefully loaded on the top of a 10-50% sucrose gradient. All tubes were equally balanced, and then the gradients were centrifuged for 3 h in SW41Ti swinging bucket rotor at 160,000 ***g*** at 4°C using a Beckman ultracentrifuge. Fractions (300 µl/tube) were collected manually and immediately transferred to an ice bucket. The absorbance was detected at 260 nm to display the polysome profile of the gradients. The proteins were precipitated with nine volumes of 96% ethanol.

Statistical analysis

All data are presented as mean±s.e.m. unless otherwise noted in the figure legends. Statistical differences between datasets were assessed using one-way ANOVA or two-tailed Student's *t*-test using the SPSS16.0 software. The Mann–Whitney *U*-test (a non-parametric statistical method) was used to analyze Fig. 3C-G. *P*-values are denoted in figures by **P*<0.05; ***P*<0.01; ****P*<0.001.

The representation factor calculation was performed to identify whether the expected number of overlaps was found between *Mnf2*-cKO and *Miwi*-KO PS and RS up- or downregulated genes using the online resource from Lund lab available at http://nemates.org/MA/progs/overlap_stats.html. A representation factor <1.0 has fewer than expected overlap, whereas a

Development (2021) 148, dev196295. doi:10.1242/dev.196295

representation factor >1.0 has more overlaps than expected. The significance of this overlap was calculated using the exact hypergeometric distribution or normal approximation of the hypergeometric distribution calculations where appropriate (Cahill et al., 2018; Fury et al., 2006; Lahiri et al., 2007). The hypergeometric distribution is similar to the one-tailed Fisher's exact test, and is commonly used to assess statistical significance of gene overlaps and/or enrichment (Fury et al., 2006; Plaisier et al., 2010). This calculation describes the expected number of successes (overlapping genes) in a series of draws from a finite population (experiment 1 genes and experiment 2 genes) without replacement (Plaisier et al., 2010). The normal approximation of the hypergeometric distribution is a method used under circumstances that the number of genes in experiment 1 (here taken to be the up-/downregulated *Mnf2*-cKO genes)×10<the total genes (total sequenced genes in PS/RS in the *Mnf2*-cKO) (Kim et al., 2001; Lahiri et al., 2007). Significance was considered to have a *P*-value<0.05.

Acknowledgements

We are grateful for engaging discussions with colleagues from Huazhong University of Science and Technology, China, in the very initial phase of the project.

Competing interests

The authors declare no competing or financial interests.

Author contributions

Conceptualization: X.W.; Methodology: X.W., Y.W., J.Z., G.S., S.G., C.C., S.A.K.; Software: G.S., S.A.K.; Validation: X.W., Y.W., S.G.; Formal analysis: X.W., Y.W., J.Z., G.S., C.C.; Investigation: X.W., Y.W., J.Z.; Resources: X.W.; Data curation: X.W.; Writing - original draft: X.W.; Writing - review & editing: S.A.K., Z.Z., S.Y.; Supervision: Z.Z., S.Y.; Project administration: S.Y.; Funding acquisition: S.Y.

Funding

This work was supported by grants from the National Natural Science Foundation of China (81971444 and 31671551 to S.Y., 31801237 to X.W.), the Science, Technology and Innovation Commission of Shenzhen Municipality (JCYJ20170244 to S.Y.) and the Natural Science Foundation of Hubei Province (2017CFA069 to S.Y.).

Data availability

All RNA-seq data have been deposited in the NCBI SRA database under the accession number SRP212036.

Supplementary information

Supplementary information available online at
https://dev.biologists.org/lookup/doi/10.1242/dev.196295.supplemental

Peer review history

The peer review history is available online at
https://journals.biologists.com/dev/article-lookup/148/7/dev196295/

References

Aboulhouda, S., Di Santo, R., Therizols, G. and Weinberg, D. (2017). Accurate, streamlined analysis of mRNA translation by sucrose gradient fractionation. *Bio. Protoc.* **7**, e2573. doi:10.21769/BioProtoc.2573

Aravin, A. A., van der Heijden, G. W., Castañeda, J., Vagin, V. V., Hannon, G. J. and Bortvin, A. (2009). Cytoplasmic compartmentalization of the fetal piRNA pathway in mice. *PLoS Genet.* **5**, e1000764. doi:10.1371/journal.pgen.1000764

Bellve, A. R. (1993). Purification, culture, and fractionation of spermatogenic cells. *Methods Enzymol.* **225**, 84-113. doi:10.1016/0076-6879(93)25009-Q

Bellve, A. R., Cavicchia, J. C., Millette, C. F., O'Brien, D. A., Bhatnagar, Y. M. and Dym, M. (1977). Spermatogenic cells of the prepuberal mouse: isolation and morphological characterization. *J. Cell Biol.* **74**, 68-85. doi:10.1083/jcb.74.1.68

Bouhy, D. and Timmerman, V. (2013). Animal models and therapeutic prospects for Charcot-Marie-Tooth disease. *Ann. Neurol.* **74**, 391-396. doi:10.1002/ana.23987

Braun, R. E. (1998). Post-transcriptional control of gene expression during spermatogenesis. *Semin. Cell Dev. Biol.* **9**, 483-489. doi:10.1006/scdb.1998.0226

Cahill, K. M., Huo, Z. G., Tseng, G. C., Logan, R. W. and Seney, M. L. (2018). Improved identification of concordant and discordant gene expression signatures using an updated rank-rank hypergeometric overlap approach. *Sci. Rep.* **8**, 9588. doi:10.1038/s41598-018-27903-2

Castañeda, J., Genzor, P., van der Heijden, G. W., Sarkeshik, A., Yates, J. R., III, Ingolia, N. T. and Bortvin, A. (2014). Reduced pachytene piRNAs and translation underlie spermiogenic arrest in Maelstrom mutant mice. *EMBO J.* **33**, 1999-2019. doi:10.15252/embj.201386855

Chen, H. and Chan, D. C. (2004). Mitochondrial dynamics in mammals. *Curr. Top. Dev. Biol.* **59**, 119-144. doi:10.1016/S0070-2153(04)59005-1

Chen, H., Detmer, S. A., Ewald, A. J., Griffin, E. E., Fraser, S. E. and Chan, D. C. (2003). Mitofusins Mfn1 and Mfn2 coordinately regulate mitochondrial fusion and are essential for embryonic development. *J. Cell Biol.* **160**, 189-200. doi:10.1083/jcb.200211046

Chen, H., McCaffery, J. M. and Chan, D. C. (2007). Mitochondrial fusion protects against neurodegeneration in the cerebellum. *Cell* **130**, 548-562. doi:10.1016/j.cell.2007.06.026

Chen, H., Vermulst, M., Wang, Y. E., Chomyn, A., Prolla, T. A., McCaffery, J. M. and Chan, D. C. (2010). Mitochondrial fusion is required for mtDNA stability in skeletal muscle and tolerance of mtDNA mutations. *Cell* **141**, 280-289. doi:10.1016/j.cell.2010.02.026

Chen, W., Sun, Y., Sun, Q., Zhang, J., Jiang, M., Chang, C., Huang, X., Wang, C., Wang, P., Zhang, Z. et al. (2020). MFN2 plays a distinct role from MFN1 in regulating spermatogonial differentiation. *Stem Cell Rep.* **14**, 803-817. doi:10.1016/j.stemcr.2020.03.024

de Brito, O. M. and Scorrano, L. (2008). Mitofusin 2 tethers endoplasmic reticulum to mitochondria. *Nature* **456**, 605-610. doi:10.1038/nature07534

Dennis, G., Jr, Sherman, B. T., Hosack, D. A., Yang, J., Gao, W., Lane, H. C. and Lempicki, R. A. (2003). DAVID: Database for Annotation, Visualization, and Integrated Discovery. *Genome Biol.* **4**, P3. doi:10.1186/gb-2003-4-5-p3

Ding, D., Liu, J., Dong, K., Melnick, A. F., Latham, K. E. and Chen, C. (2019). Mitochondrial membrane-based initial separation of MIWI and MILI functions during pachytene piRNA biogenesis. *Nucleic Acids Res.* **47**, 2594-2608. doi:10.1093/nar/gky1281

Doiguchi, M., Mori, T., Toshimori, K., Shibata, Y. and Iida, H. (2002). Spergen-1 might be an adhesive molecule associated with mitochondria in the middle piece of spermatozoa. *Dev. Biol.* **252**, 127-137. doi:10.1006/dbio.2002.0833

Dong, J., Wang, X., Cao, C., Wen, Y., Sakashita, A., Chen, S., Zhang, J., Zhang, Y., Zhou, L., Luo, M. et al. (2019). UHRF1 suppresses retrotransposons and cooperates with PRMT5 and PIWI proteins in male germ cells. *Nat. Commun.* **10**, 4705. doi:10.1038/s41467-019-12455-4

Eddy, E. M. (1970). Cytochemical observations on the chromatoid body of the male germ cells. *Biol. Reprod.* **2**, 114-128. doi:10.1095/biolreprod2.1.114

Eddy, E. M. (1974). Fine structural observations on the form and distribution of nuage in germ cells of the rat. *Anat. Rec.* **178**, 731-757. doi:10.1002/ar.1091780406

Eddy, E. M. (1975). Germ plasm and the differentiation of the germ cell line. *Int. Rev. Cytol.* **43**, 229-280. doi:10.1016/S0074-7696(08)60070-4

Fanourgakis, G., Lesche, M., Akpinar, M., Dahl, A. and Jessberger, R. (2016). Chromatoid body protein TDRD6 supports long 3′ UTR triggered nonsense mediated mRNA decay. *PLoS Genet.* **12**, e1005857. doi:10.1371/journal.pgen.1005857

Fawcett, D. W., Eddy, E. M. and Phillips, D. M. (1970). Observations on the fine structure and relationships of the chromatoid body in mammalian spermatogenesis. *Biol. Reprod.* **2**, 129-153. doi:10.1095/biolreprod2.1.129

Fury, W., Batliwalla, F., Gregersen, P. K. and Li, W. (2006). Overlapping probabilities of top ranking gene lists, hypergeometric distribution, and stringency of gene selection criterion. *Conf. Proc. IEEE Eng. Med. Biol. Soc.* **2006**, 5531-5534. doi:10.1109/IEMBS.2006.260828

Goh, W. S. S., Falciatori, I., Tam, O. H., Burgess, R., Meikar, O., Kotaja, N., Hammell, M. and Hannon, G. J. (2015). piRNA-directed cleavage of meiotic transcripts regulates spermatogenesis. *Genes Dev.* **29**, 1032-1044. doi:10.1101/gad.260455.115

Grivna, S. T., Pyhtila, B. and Lin, H. (2006). MIWI associates with translational machinery and PIWI-interacting RNAs (piRNAs) in regulating spermatogenesis. *Proc. Natl. Acad. Sci. USA* **103**, 13415-13420. doi:10.1073/pnas.0605506103

Gu, W., Tekur, S., Reinbold, R., Eppig, J. J., Choi, Y.-C., Zheng, J. Z., Murray, M. T. and Hecht, N. B. (1998). Mammalian male and female germ cells express a germ cell-specific Y-Box protein, MSY21. *Biol. Reprod.* **59**, 1266-1274. doi:10.1095/biolreprod59.5.1266

Hales, K. G. and Fuller, M. T. (1997). Developmentally regulated mitochondrial fusion mediated by a conserved, novel, predicted GTPase. *Cell* **90**, 121-129. doi:10.1016/S0092-8674(00)80319-0

Hou, X., Zhu, S., Zhang, H., Li, C., Qiu, D., Ge, J., Guo, X. and Wang, Q. (2019). Mitofusin1 in oocyte is essential for female fertility. *Redox Biol.* **21**, 101110. doi:10.1016/j.redox.2019.101110

Jiang, M., Kauppila, T. E. S., Motori, E., Li, X., Atanassov, I., Folz-Donahue, K., Bonekamp, N. A., Albarran-Gutierrez, S., Stewart, J. B. and Larsson, N.-G. (2017). Increased total mtDNA copy number cures male infertility despite unaltered mtDNA mutation load. *Cell Metab.* **26**, 429-436.e424. doi:10.1016/j.cmet.2017.07.003

Karamysheva, Z. N., Tikhonova, E. B., Grozdanov, P. N., Huffman, J. C., Baca, K. R., Karamyshev, A., Denison, R. B., MacDonald, C. C., Zhang, K. and Karamyshev, A. L. (2018). Polysome profiling in leishmania, human cells and mouse testis. *J. Vis. Exp.* **134**, 57600. doi:10.3791/57600

Kim, S. K., Lund, J., Kiraly, M., Duke, K., Jiang, M., Stuart, J. M., Eizinger, A., Wylie, B. N. and Davidson, G. S. (2001). A gene expression map for Caenorhabditis elegans. *Science* **293**, 2087-2092. doi:10.1126/science.1061603

Kleene, K. C. (2013). Connecting cis-elements and trans-factors with mechanisms of developmental regulation of mRNA translation in meiotic and haploid mammalian spermatogenic cells. *Reproduction* **146**, R1-R19. doi:10.1530/REP-12-0362

Kotaja, N. and Sassone-Corsi, P. (2007). The chromatoid body: a germ-cell-specific RNA-processing centre. *Nat. Rev. Mol. Cell Biol.* **8**, 85-90. doi:10.1038/nrm2081

Lahiri, S. N., Chatterjee, A. and Maiti, T. (2007). Normal approximation to the hypergeometric distribution in nonstandard cases and a sub-Gaussian Berry-Esseen theorem. *J. Stat. Plan Infer.* **137**, 3570-3590. doi:10.1016/j.jspi.2007.03.033

Larriba, E. and Del Mazo, J. (2018). An integrative piRNA analysis of mouse gametes and zygotes reveals new potential origins and gene regulatory roles. *Sci. Rep.* **8**, 12832. doi:10.1038/s41598-018-31032-1

Ma, L., Buchold, G. M., Greenbaum, M. P., Roy, A., Burns, K. H., Zhu, H., Han, D. Y., Harris, R. A., Coarfa, C., Gunaratne, P. H. et al. (2009). GASZ is essential for male meiosis and suppression of retrotransposon expression in the male germline. *PLoS Genet.* **5**, e1000635. doi:10.1371/journal.pgen.1000635

Matsumoto, K. and Wolffe, A. P. (1998). Gene regulation by Y-box proteins: coupling control of transcription and translation. *Trends Cell Biol.* **8**, 318-323. doi:10.1016/S0962-8924(98)01300-2

Matsuoka, Y., Iguchi, N., Kitamura, K., Nishimura, H., Manabe, H., Miyagawa, Y., Koga, M., Matsumiya, K., Okuyama, A., Tanaka, H. et al. (2004). Cloning and characterization of a mouse spergen-1 localized in sperm mitochondria. *Int. J. Androl.* **27**, 152-160. doi:10.1111/j.1365-2605.2004.00466.x

Mi, Y., Shi, Z. and Li, J. (2015). Spata19 is critical for sperm mitochondrial function and male fertility. *Mol. Reprod. Dev.* **82**, 907-913. doi:10.1002/mrd.22536

Misko, A. L., Sasaki, Y., Tuck, E., Milbrandt, J. and Baloh, R. H. (2012). Mitofusin2 mutations disrupt axonal mitochondrial positioning and promote axon degeneration. *J. Neurosci.* **32**, 4145-4155. doi:10.1523/JNEUROSCI.6338-11.2012

Nagamori, I., Cruickshank, V. A. and Sassone-Corsi, P. (2011). Regulation of an RNA granule during spermatogenesis: acetylation of MVH in the chromatoid body of germ cells. *J. Cell Sci.* **124**, 4346-4355. doi:10.1242/jcs.096461

Naon, D., Zaninello, M., Giacomello, M., Varanita, T., Grespi, F., Lakshminaranayan, S., Serafini, A., Semenzato, M., Herkenne, S., Hernández-Alvarez, M. I. et al. (2016). Critical reappraisal confirms that Mitofusin 2 is an endoplasmic reticulum-mitochondria tether. *Proc. Natl. Acad. Sci. USA* **113**, 11249-11254. doi:10.1073/pnas.1606786113

Paillusson, S., Stoica, R., Gomez-Suaga, P., Lau, D. H. W., Mueller, S., Miller, T. and Miller, C. C. J. (2016). There's something wrong with my MAM; the ER-mitochondria axis and neurodegenerative diseases. *Trends Neurosci.* **39**, 146-157. doi:10.1016/j.tins.2016.01.008

Palmer, C. S., Osellame, L. D., Stojanovski, D. and Ryan, M. T. (2011). The regulation of mitochondrial morphology: intricate mechanisms and dynamic machinery. *Cell. Signal.* **23**, 1534-1545. doi:10.1016/j.cellsig.2011.05.021

Plaisier, S. B., Taschereau, R., Wong, J. A. and Graeber, T. G. (2010). Rank-rank hypergeometric overlap: identification of statistically significant overlap between gene-expression signatures. *Nucleic Acids Res.* **38**, e169. doi:10.1093/nar/gkq636

Poston, C. N., Krishnan, S. C. and Bazemore-Walker, C. R. (2013). In-depth proteomic analysis of mammalian mitochondria-associated membranes (MAM). *J. Proteomics* **79**, 219-230. doi:10.1016/j.jprot.2012.12.018

Ren, M., Xu, Y., Erdjument-Bromage, H., Donelian, A., Phoon, C. K. L., Terada, N., Strathdee, D., Neubert, T. A. and Schlame, M. (2019). Extramitochondrial cardiolipin suggests a novel function of mitochondria in spermatogenesis. *J. Cell Biol.* **218**, 1491-1502. doi:10.1083/jcb.201808131

Rieusset, J. (2018). The role of endoplasmic reticulum-mitochondria contact sites in the control of glucose homeostasis: an update. *Cell Death Dis.* **9**, 388. doi:10.1038/s41419-018-0416-1

Ross, J. M. (2011). Visualization of mitochondrial respiratory function using cytochrome c oxidase/succinate dehydrogenase (COX/SDH) double-labeling histochemistry. *J. Vis. Exp.* **57**, e3266. doi:10.3791/3266

Rouzier, C., Bannwarth, S., Chaussenot, A., Chevrollier, A., Verschueren, A., Bonello-Palot, N., Fragaki, K., Cano, A., Pouget, J., Pellissier, J.-F. et al. (2012). The MFN2 gene is responsible for mitochondrial DNA instability and optic atrophy 'plus' phenotype. *Brain* **135**, 23-34. doi:10.1093/brain/awr323

Sadate-Ngatchou, P. I., Payne, C. J., Dearth, A. T. and Braun, R. E. (2008). Cre recombinase activity specific to postnatal, premeiotic male germ cells in transgenic mice. *Genesis* **46**, 738-742. doi:10.1002/dvg.20437

Santel, A. and Fuller, M. T. (2001). Control of mitochondrial morphology by a human mitofusin. *J. Cell Sci.* **114**, 867-874.

Sassone-Corsi, P. (2002). Unique chromatin remodeling and transcriptional regulation in spermatogenesis. *Science* **296**, 2176-2178. doi:10.1126/science.1070963

Saxe, J. P., Chen, M., Zhao, H. and Lin, H. (2013). Tdrkh is essential for spermatogenesis and participates in primary piRNA biogenesis in the germline. *EMBO J.* **32**, 1869-1885. doi:10.1038/emboj.2013.121

Schneeberger, M., Dietrich, M. O., Sebastián, D., Imbernón, M., Castaño, C., Garcia, A., Esteban, Y., Gonzalez-Franquesa, A., Rodríguez, I. C., Bortolozzi, A. et al. (2013). Mitofusin 2 in POMC neurons connects ER stress with leptin resistance and energy imbalance. *Cell* **155**, 172-187. doi:10.1016/j.cell.2013.09.003

Shen, S., Park, J. W., Lu, Z.-X., Lin, L., Henry, M. D., Wu, Y. N., Zhou, Q. and Xing, Y. (2014). rMATS: robust and flexible detection of differential alternative splicing from replicate RNA-Seq data. *Proc. Natl. Acad. Sci. USA* **111**, E5593-E5601. doi:10.1073/pnas.1419161111

Soper, S. F. C., van der Heijden, G. W., Hardiman, T. C., Goodheart, M., Martin, S. L., de Boer, P. and Bortvin, A. (2008). Mouse maelstrom, a component of nuage, is essential for spermatogenesis and transposon repression in meiosis. *Dev. Cell* **15**, 285-297. doi:10.1016/j.devcel.2008.05.015

Takebe, M., Onohara, Y. and Yokota, S. (2013). Expression of MAEL in nuage and non-nuage compartments of rat spermatogenic cells and colocalization with DDX4, DDX25 and MIWI. *Histochem. Cell Biol.* **140**, 169-181. doi:10.1007/s00418-012-1067-4

Theurey, P., Tubbs, E., Vial, G., Jacquemetton, J., Bendridi, N., Chauvin, M.-A., Alam, M. R., Le Romancer, M., Vidal, H. and Rieusset, J. (2016). Mitochondria-associated endoplasmic reticulum membranes allow adaptation of mitochondrial metabolism to glucose availability in the liver. *J. Mol. Cell Biol.* **8**, 129-143. doi:10.1093/jmcb/mjw004

Toyooka, Y., Tsunekawa, N., Takahashi, Y., Matsui, Y., Satoh, M. and Noce, T. (2000). Expression and intracellular localization of mouse Vasa-homologue protein during germ cell development. *Mech. Dev.* **93**, 139-149. doi:10.1016/S0925-4773(00)00283-5

van der Heijden, G. W., Castañeda, J. and Bortvin, A. (2010). Bodies of evidence—compartmentalization of the piRNA pathway in mouse fetal prospermatogonia. *Curr. Opin. Cell Biol.* **22**, 752-757. doi:10.1016/j.ceb.2010.08.014

Varuzhanyan, G., Rojansky, R., Sweredoski, M. J., Graham, R. L. J., Hess, S., Ladinsky, M. S. and Chan, D. C. (2019). Mitochondrial fusion is required for spermatogonial differentiation and meiosis. *eLife* **8**, e51601. doi:10.7554/eLife.51601

Vasileva, A., Tiedau, D., Firooznia, A., Müller-Reichert, T. and Jessberger, R. (2009). Tdrd6 is required for spermiogenesis, chromatoid body architecture, and regulation of miRNA expression. *Curr. Biol.* **19**, 630-639. doi:10.1016/j.cub.2009.02.047

Wang, X., Wen, Y., Dong, J., Cao, C. and Yuan, S. (2018). Systematic in-depth proteomic analysis of mitochondria-associated endoplasmic reticulum membranes in mouse and human testes. *Proteomics* **18**, e1700478. doi:10.1002/pmic.201700478

Wang, X., Lv, C., Guo, Y. and Yuan, S. (2020). Mitochondria associated germinal structures in spermatogenesis: piRNA pathway regulation and beyond. *Cells* **9**, 399. doi:10.3390/cells9020399

Westermann, B. (2010). Mitochondrial fusion and fission in cell life and death. *Nat. Rev. Mol. Cell Biol.* **11**, 872-884. doi:10.1038/nrm3013

Wykes, S. M. and Krawetz, S. A. (2003). The structural organization of sperm chromatin. *J. Biol. Chem.* **278**, 29471-29477. doi:10.1074/jbc.M304545200

Xu, M. and Hecht, N. B. (2008). MSY2 and polypyrimidine tract binding protein 2 stabilize mRNAs in the mammalian testis. *Int. J. Androl.* **31**, 457-461. doi:10.1111/j.1365-2605.2008.00885.x

Yang, J., Medvedev, S., Reddi, P. P., Schultz, R. M. and Hecht, N. B. (2005a). The DNA/RNA-binding protein MSY2 marks specific transcripts for cytoplasmic storage in mouse male germ cells. *Proc. Natl. Acad. Sci. USA* **102**, 1513-1518. doi:10.1073/pnas.0404685102

Yang, J., Medvedev, S., Yu, J., Tang, L. C., Agno, J. E., Matzuk, M. M., Schultz, R. M. and Hecht, N. B. (2005b). Absence of the DNA-/RNA-binding protein MSY2 results in male and female infertility. *Proc. Natl. Acad. Sci. USA* **102**, 5755-5760. doi:10.1073/pnas.0408718102

Yang, J., Morales, C. R., Medvedev, S., Schultz, R. M. and Hecht, N. B. (2007). In the absence of the mouse DNA/RNA-binding protein MSY2, messenger RNA instability leads to spermatogenic arrest. *Biol. Reprod.* **76**, 48-54. doi:10.1095/biolreprod.106.055095

Zhang, P., Kang, J.-Y., Gou, L.-T., Wang, J., Xue, Y., Skogerboe, G., Dai, P., Huang, D.-W., Chen, R., Fu, X.-D. et al. (2015). MIWI and piRNA-mediated cleavage of messenger RNAs in mouse testes. *Cell Res.* **25**, 193-207. doi:10.1038/cr.2015.4

Zhang, J., Wang, Q., Wang, M., Jiang, M., Wang, Y., Sun, Y., Wang, J., Xie, T., Tang, C., Tang, N. et al. (2016). GASZ and mitofusin-mediated mitochondrial functions are crucial for spermatogenesis. *EMBO Rep.* **17**, 220-234. doi:10.15252/embr.201540846

Züchner, S., Mersiyanova, I. V., Muglia, M., Bissar-Tadmouri, N., Rochelle, J., Dadali, E. L., Zappia, M., Nelis, E., Patitucci, A., Senderek, J. et al. (2004). Mutations in the mitochondrial GTPase mitofusin 2 cause Charcot-Marie-Tooth neuropathy type 2A. *Nat. Genet.* **36**, 449-451. doi:10.1038/ng1341